Article:
Stavrou, AG, Hare, C, Hassanpour, A orcid.org/0000-0002-7756-1506 et al. (1 more author) (2020) Investigation of powder flowability at low stresses: Influence of particle size and size distribution. Powder Technology, 364. pp. 98-114. ISSN 0032-5910

https://doi.org/10.1016/j.powtec.2020.01.068

Investigation of powder flowability at low stresses: Influence of particle size and size distribution

Alexandros Georgios Stavrou [a], Colin Hare [a,*], Ali Hassanpour [b], Chuan-Yu Wu [a]

[a] Department of Chemical and Process Engineering, Faculty of Engineering and Physical Sciences, University of Surrey, Guildford, GU2 7XH, UK

[b] School of Chemical and Process Engineering, Faculty of Engineering, University of Leeds, Leeds, LS2 9JT, UK

* Corresponding author: telephone number: +44 (0)1483 689472, e-mail address: c.hare@surrey.ac.uk

ABSTRACT

At moderate stresses, shear cells are the preferred method of powder flow measurement. However, several industrial processes operate at low stresses, where the determination of unconfined yield strength by the shear cell technique may be inconsistent, or found not to correlate with observed behaviour. Alternatively, ball indentation can be used, which directly measures hardness; related to unconfined yield strength by the constraint factor. However, it is not known how constraint factor is influenced by particle properties. Here, ball indentation and shear cell methods are applied for glass beads of various size distributions, and the influence of particle size distribution on the constraint factor is explored. The constraint factor is shown to be independent of the pre-consolidation stress, though reduces as the d_{10}, d_{50} or d_{90} are increased. Unconfined yield strength inferred from indentation measurements suggest that extrapolation of shear cell data to low stresses overestimates the unconfined yield strength.

Keywords:

Powder flowability

Low consolidation stresses

Ball indentation

Shear cell

Particle size

Particle size distribution

1 Introduction

Numerous industries such as pharmaceuticals, food and fast-moving consumer goods often handle materials in the form of powders. Reliable and consistent prediction of the flow behaviour of the powders can be very challenging, especially when the powders are cohesive. Cohesive materials can lead to the formation of stagnant regions or flow stoppages in process equipment, resulting in uncontrolled or erratic flow rates from industrial equipment, and potentially causing segregation problems [1]. Powder flow is not an inherent material property, being dependent on material physical properties, process conditions and environmental conditions [2].

Particle size and its distribution is one of the most influential properties on powder flow. For a given powder, reducing particle size tends to reduce flowability [3-9], because the particle surface area per unit mass increases as particle size decreases, providing a greater surface area for surface cohesive forces to interact, and therefore resulting in a more cohesive flow behaviour [10]. However, powders with similar size can exhibit different flow behaviours due to differences in other properties such as particle morphology and surface roughness [11,12]. Larger particles pack more efficiently due to the ease with which they flow past one another to fill voids in the bed, while as the particle size decreases flowability deteriorates and particles pack more loosely [13]. Cohesion becomes increasingly important as the particle size decreases, especially for powders that are very fine e.g. <

50 µm, since the interparticle forces are significant in comparison with the weight of the particles [14]. Though it should be noted that this threshold depends on other particle properties such as density, shape and roughness.

The effect of the particle size distribution within a mixture is more complex. Lumay *et al.* [14] tested five flour powders, finding that as the size distribution becomes narrower, and at the same time the d_{10} becomes larger, flowability improves. Abdullah and Geldart [15] examined the packing of binary mixtures of coarse and fine particles in aerated and tapped states, with their findings being easily translatable to powder flow behaviour. In the case of aerated mixtures, the poured density initially increased with a reduction in fines content, eventually reaching a plateau. On the other hand, for the tapped system the tapped density initially increased with a reduction in fines content, and then decreased since insufficient small particles were available to fill the voids in between the larger particles. The Hausner ratio exhibited a continuous decrease with a reduction in fines content, indicating an improvement in flowability. Gold *et al.* [16] showed that when fine particles are added to lactose granules, the flowrate of the mixture increases with an increase in the amount of fine particles until a given maximum flowrate is achieved. However, when this maximum is reached, any increase in the amount of fine particles results in a decrease in the flowability of the mixture. In addition, their finding shows that the quantity of fine particles required to reach the maximum flowrate for a given material decreases with a reduction of the size of the fines. Liu *et al.* [17] showed that when the finest particles of a needle-shaped ibuprofen powder are separated from the bulk, the fine powders flow better than the bulk powder. This is attributed to the narrower size distribution.

The flowability of a powder is generally improved by inclusion of larger particles and worsened by the inclusion of finer particles. This means that the influence of widening size distribution on the powder flowability can be difficult to predict [18]. Molerus and Nwylt [19] found that for binary mixtures of coarse and fine limestone particles, an increase in the fines content results in an increase

in the unconfined yield strength, eventually becoming equal to the strength of the fines alone once a fines content of 30 % w/w is reached. At fines contents equal or greater than this it is expected that the coarse particles are completely embedded by the fines, and so the flow behaviour is governed by the interparticle forces between the fines. In a binary mixture of coarse and fine particles, contacts between coarse particles dominate flow behaviour when the fines content is small, while contacts between fine particles dominate when the fines content is large, with the coarse-fine contacts not seen to dominate at any fines content [20].

Reliable prediction of powder flow based solely on particle properties is not yet possible, due to the complexity of powder systems. However, a large number of techniques have been developed for evaluating powder flowability, thus enabling the decoupling of the contribution of particle size, among other parameters, on granular flow. None of these techniques are applicable across a full range of applied stresses and strain rates though, and therefore consideration needs to be given for the measurement technique to be used for each circumstance. However, shear cells are the most well-established flowability measurement method, and are readily used for silo and hopper design [21,22]. Shear cells determine the onset of powder flow in a quasi-static manner, measuring the shear stress required to initiate flow under a given normal stress, and subsequently allowing the unconfined yield strength to be estimated from the measured yield locus. Shear cells typically operate under moderate to high stresses, and like the majority of powder testers often fail to reliably assess powder flowability at low consolidation stresses (≤ 1 kPa). At such stresses shear cells are normally unable to generate steady-state shear, or the reproducibility of the measurement of unconfined yield strength is greatly reduced, or does not correlate with observed process behaviour [23,24]. Flow behaviour at low stresses may be estimated from shear testing at higher stresses by assuming linearity of the yield loci, and extrapolating towards zero normal stress. However, this leads to an overestimation of unconfined yield strength and cohesion, since yield loci tend to deviate sharply from the linear regression in the region of low stresses [23].

There are many industrial processes during which granular materials are subjected to low stresses, such as die filling and dosing of powders in capsules. Under such stresses, small contact areas exist between constituent particles, and very little particle deformation occurs, leading to a low structural strength [25]. In order to address the need for reliable methods to measure flow resistance of weakly consolidated powders, ball indentation (BI) was introduced by Hassanpour and Ghadiri [26], with its operational window being thoroughly established experimentally by Zafar *et al.* [27] and computationally by Pasha *et al.* [28]. In this technique a die, made of low friction material, is filled with powder and pre-consolidated by uniaxial compression with a piston, which is then unloaded. Following this, a spherical indenter is driven into the sample, whilst its penetration depth and the resulting vertical force are measured until a desired depth is reached, and then the indenter is unloaded (Fig. 1).

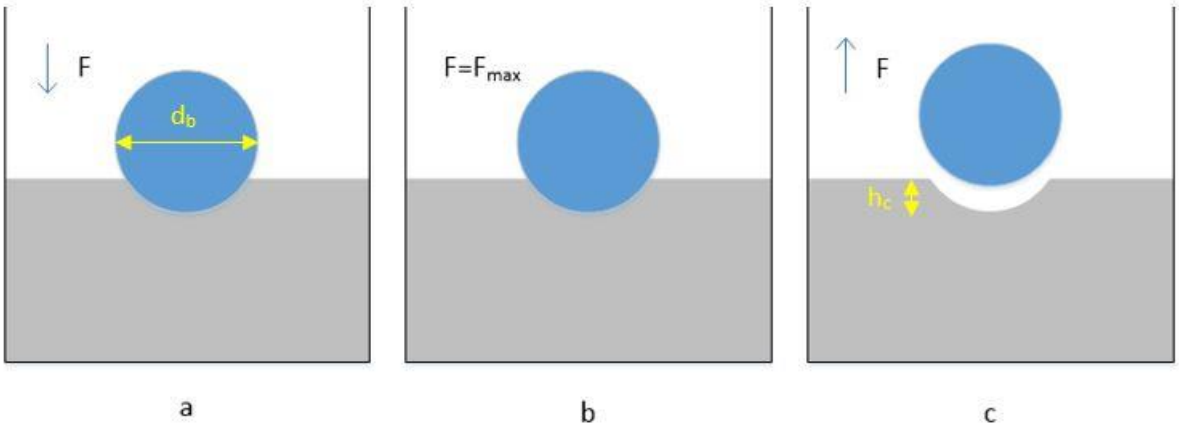

Fig. 1. Indentation step [29].

From the force-displacement response of the powder bed, the hardness of the material is directly measured via Eq. (1), which corresponds to the resistance of the bed to plastic deformation.

$$H = F_{max}/A \quad (1)$$

where F_{max} is the maximum indentation load and A is the projected area of the impression of the indenter, calculated from Eq. (2):

115 $$A = \pi\left(d_b h_c - {h_c}^2\right) \quad (2)$$

116 where d_b is the indenter diameter and h_c is the indent depth after unloading. If unloading has
117 negligible effect on the material's recovery, the penetration depth at maximum indentation load can
118 be used in place of h_c [26].

119 Ball indentation can be applied as long as the powder compact has a relatively flat surface, which is
120 typically achieved at pre-consolidation stresses as low as 100 Pa. It therefore offers the capability of
121 obtaining hardness measurements at any stress level above this. However, it is commonly of interest
122 to measure the unconfined yield strength, as measured by uniaxial compression tests, or determined
123 in a shear cell. Tabor [30] demonstrated for continuum materials that hardness is directly linked to
124 the unconfined yield strength, σ_c, via Eq. (3):

125 $$H = C\,\sigma_c \quad (3)$$

126 where C is the constraint factor. The constraint factor represents the additional resistance caused by
127 an elastically deforming region around the plastically deforming indentation zone. This leads to an
128 increase in the local yield strength, represented by the hardness [31]. This has also been observed in
129 particulate systems [26,32]. In the case of continuum solids, the constraint factor has been stated to
130 have a value of 3 for rigid-perfectly plastic materials [33], while according to Tabor [30] this value is
131 applicable only for ductile metals. Furthermore, for continuum materials C is known to depend on
132 material properties [34]. Johnson [35] introduced a relationship between indentation hardness and
133 yield strength for elastic-perfectly plastic materials, based on Young's modulus, radius of the
134 impression, and the indenter radius. For particle systems the constraint factor doesn't have a fixed
135 value, with different values determined for a variety of powders [26,32,36]. Currently the constraint
136 factor of a powder is not known *a priori*, nor is it known which particle properties influence C, and to
137 what extent. Shedding light on all of the above is of particular importance because it will render it
138 possible for Eq. (3) to be utilised to infer unconfined yield strength from ball indentation
139 measurements at low stresses, which otherwise cannot be easily determined [32].

The aim of this study is to measure powder flowability using shear cell testing and ball indentation in order to determine how powder flowability at low stresses (≤ 1 kPa) differs from that at high stresses, and to investigate the influence of particle size and size distribution on powder flowability and the constraint factor. Furthermore, the reliability of both techniques at low stress levels is evaluated.

2 Materials and methods

In this study, glass beads supplied by Sigmund Lindner GmbH (Germany) are tested as a model material, due to their high sphericity and availability in a wide range of sizes. For each experimental series, a set of samples is prepared which vary by one parameter: median particle size, width of size distribution, d_{10}, or d_{90}. Glass beads were sieved using British Standard sieves to produce five consecutive single sieve cuts of 45 - 53, 53 - 63, 63 - 75, 75 - 90 and 90 - 106 µm, for the study of the influence of particle size on the flow behaviour. Furthermore, by mixing the above single sieve cuts, wider size distributions were created to study the influence of the width of the size distribution on flowability. A 53 - 90 µm mixture was created by mixing 50 % w/w of the 63 - 75 µm single sieve cut and 25 % w/w of each of the 53 - 63 and 75 - 90 µm single sieve cuts, while a 45 - 106 µm mixture was created by mixing 40 % w/w of the 63 - 75 µm sieve cut, 20 % w/w of each of the 53 - 63 and 75 - 90 µm sieve cuts, and 10 % w/w of each of the 45 - 53 and 90 - 106 µm sieve cuts. Moreover, the median single sieve cut of 63 - 75 µm was mixed with fractions of fine and coarse particles to investigate the influence of the shift of d_{10} and d_{90}, respectively, on powder flowability. In this case, the coarse particles are from a 150 - 180 µm sieve cut and the fine particles are from an as received '0 - 20 µm' batch. Mixtures consisting of 90 % w/w 63 - 75 µm and 10 % w/w coarse/fine particles and others having 80 % w/w 63 - 75 µm and 20 % w/w coarse/fines were created. All mixtures were created by mixing in a TURBULA T2C Shaker-Mixer at 49 rpm for 45 mins.

Particle characterisation of all aforementioned samples was conducted by dynamic image analysis using the QICPIC (Sympatec, Germany) system with the GRADIS dry dispersion mode, except for the

mixtures of 90 % w/w 63 - 75 µm with 10 % w/w fines and 80 % w/w 63 - 75 µm with 20 % w/w fines that were analysed by laser diffraction using the Mastersizer 2000 (Malvern Panalytical, UK), since the fines were too small to be analysed using the QICPIC. The size distributions of the consecutive single sieve cuts, the wider size distribution mixtures, the mixtures with coarse particles and the mixtures with fines are presented in Figs. 2, 3, 4 and 5, respectively. Shape characterisation of the samples was carried out with the QICPIC and is shown in Table 1, along with the size data for all samples.

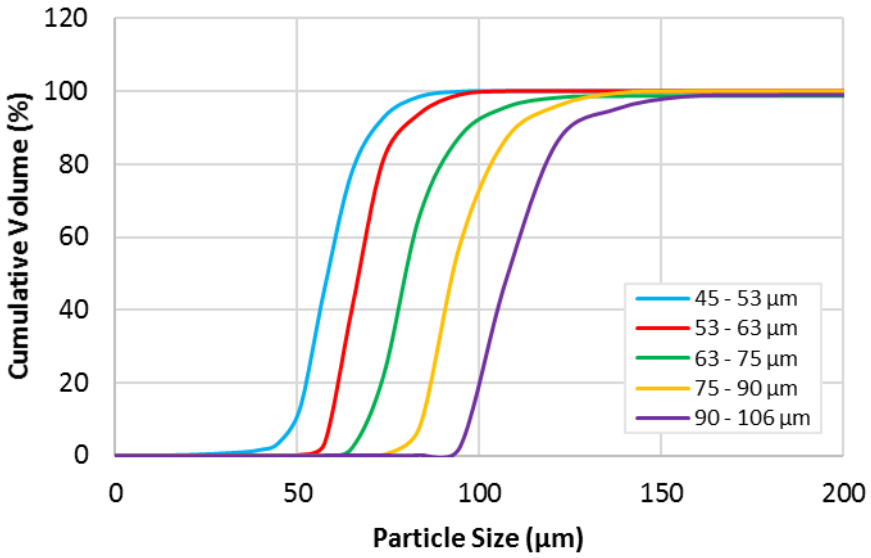

Fig. 2. Size distributions of glass bead single sieve cuts.

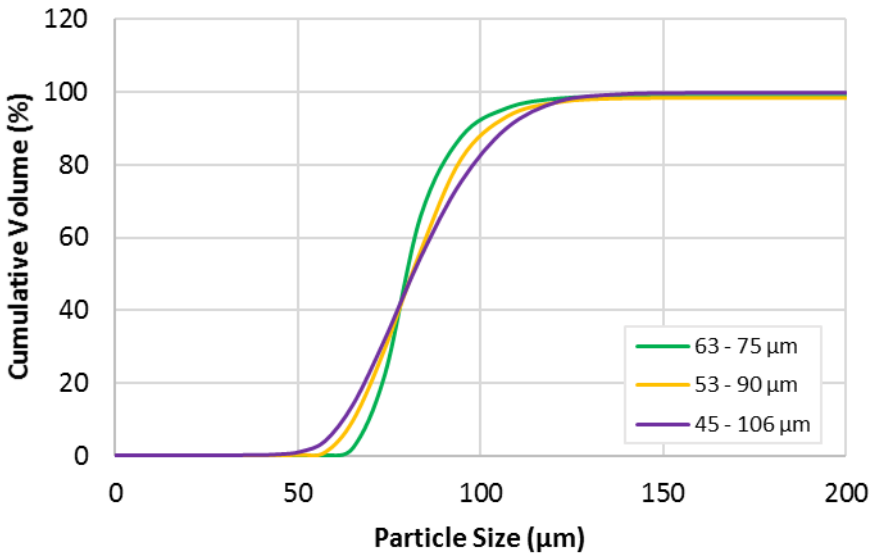

175

176 **Fig. 3.** Size distributions of glass bead wider distribution mixtures.

177

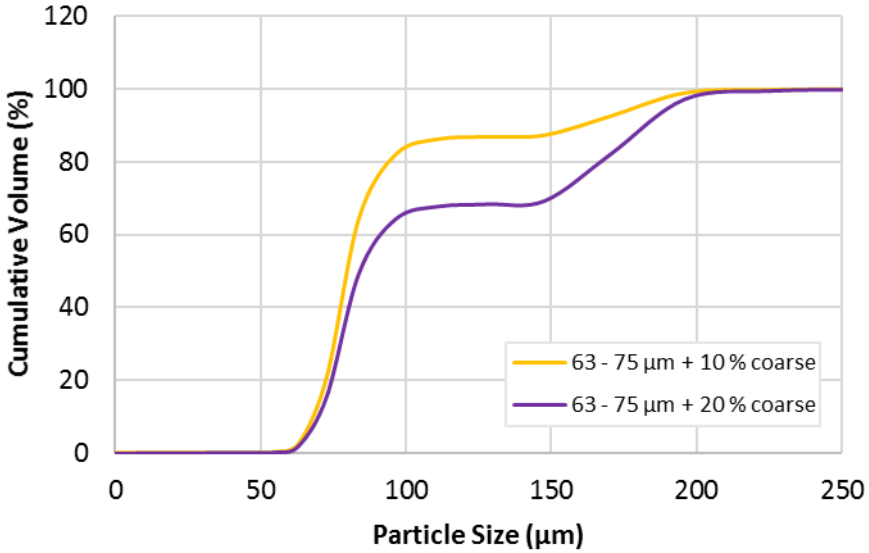

178

179 **Fig. 4.** Size distributions of glass bead mixtures with coarse particles.

180

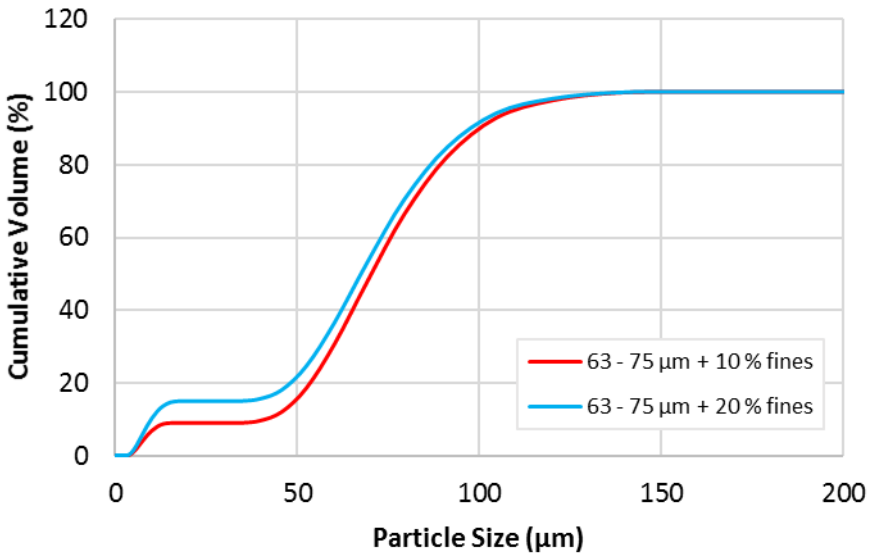

Fig. 5. Size distributions of glass bead mixtures with fines.

Table 1. Material characterisation overview.

Material	d_{10}	d_{50}	d_{90}	Span $[(d_{90}-d_{10})/d_{50}]$	Sphericity	AR (width/length)
45 - 53 µm glass beads#	48.9	58.4	72.1	0.40	0.91	0.85
53 - 63 µm glass beads#	58.8	67	80.5	0.32	0.92	0.88
63 - 75 µm glass beads#	68.3	79.9	98	0.37	0.92	0.89
75 - 90 µm glass beads#	84	92.9	112.1	0.30	0.93	0.91
90 - 106 µm glass beads#	96.7	108	128.3	0.29	0.93	0.92
53 - 90 µm glass beads#	65.1	81.2	103.5	0.47	0.92	0.89
45 - 106 µm glass beads#	61.9	81.5	106.8	0.55	0.92	0.88
63 - 75 µm + 10 % coarse glass beads#	67	80.1	159.3	1.15	0.93	0.9
63 - 75 µm + 20 % coarse glass beads#	68.7	84.4	183.5	1.36	0.93	0.91
63 - 75 µm + 10 % fine glass beads##	41	70.1	99.7	0.84	-	-
63 - 75 µm + 20 % fine glass beads##	9.8	67.5	97.5	1.30	-	-

Size measurement by QICPIC (GRADIS)
Size measurement by Mastersizer

All samples of glass beads were then silanised in order to make them cohesive. The commercially available Sigmacote® silane solution supplied by Merck (Germany) was used for the surface treatment. Sigmacote® is 1,7-Dichloro-1,1,3,3,5,5,7,7-octamethyltetrasiloxane in Heptane solution. A 50 - 75 g sample of powder (depending on particle size) was submerged in Sigmacote® for 30 minutes and the excess solution was removed by vacuum filtration for reuse. This step was repeated three times in total. Then, the solids were washed with de-ionised water in order to remove the

hydrochloric acid by-product of the reaction. The water was then removed and the coated samples were left in the oven overnight to dry at 50 ^{o}C.

The flowability of all samples was measured both by shear cell testing and ball indentation. First, in order to determine the unconfined yield strength of the materials, shear testing was carried out using the cylindrical shear cell attachment of the FT4 Powder Rheometer (Freeman Technology, UK). The principles of shear testing are covered extensively in literature, and can be found elsewhere [23]. For each sample, tests at 2, 4, 6 and 8 kPa pre-shear normal stress (σ_{pre}) were carried out. In addition to this, in the case of the 45 - 53 µm sample, additional shear tests were performed at low pre-shear normal stresses of 0.06, 0.1, 0.25, 0.5 and 1 kPa. A pre-shear normal stress of 0.06 kPa represents the lowest possible stress in the FT4 that will allow five unique, lower values of target applied normal stress to be given. In each case, the target normal stresses were chosen by trial and error, so that they are distributed approximately equidistantly and the point of incipient flow with the lowest normal stress is located close to, but at a higher stress than the tangency point of the yield locus to the failure Mohr circle. This approach is followed to minimise extrapolation of the yield locus in order for the failure Mohr circle to be constructed, which would lead to increased uncertainty when determining the unconfined yield strength [23]. The desired range of normal stresses for shear to failure is covered extensively by Schulze [23]. As a result of this approach, the target normal stresses that were chosen to be applied in the shear tests varied for each of the materials tested.

At each pre-shear normal stress the shear cell software takes the measured shear stress at each normal stress to generate the yield locus for this packing state. By default the FT4 software applies a linear fit to the measured points, followed by application of Mohr circle analysis to allow the major principal stress, σ_1, the unconfined yield strength, σ_c, and subsequently the flow function coefficient, ff_c, to be determined for each pre-shear normal stress. However, it was found that in many cases the

measured yield locus was not tangent to the constructed failure Mohr circle, but cut through the circle, as shown in Fig. 6, therefore the unconfined yield strength was overestimated.

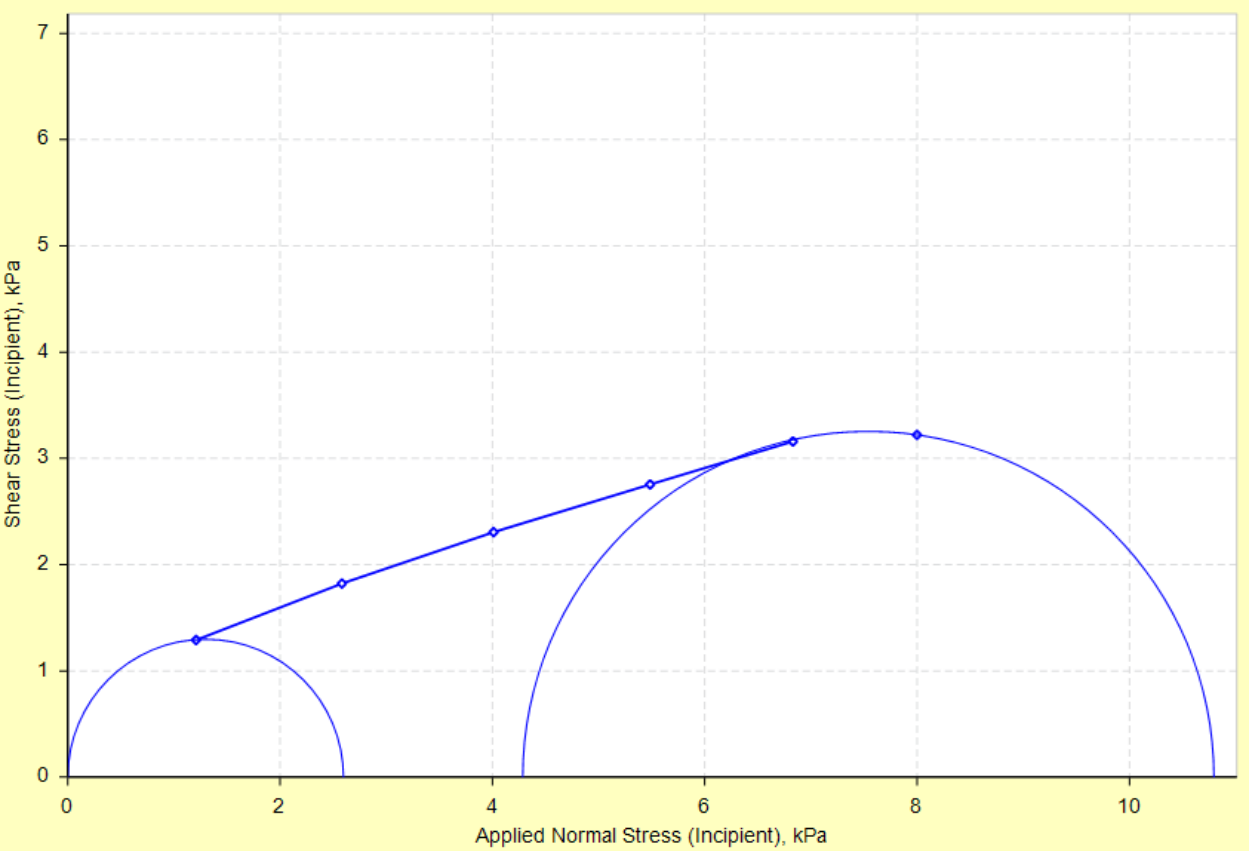

Fig. 6. Yield locus automatically generated by the FT4 software at σ_{pre} = 8 kPa.

In order to address this issue, the Warren Spring model [37] was employed for the characterisation of the yield locus using a MATLAB code provided by Dr. Massih Pasha (The Chemours Company, USA). A representative example of the Warren Spring fit to the same experimental data as in Fig. 6 is shown in Fig. 7. The pre-shear point was not considered for the fitting, to avoid the extra curvature to the yield locus and a reduction of the estimated major principal stress that its inclusion would cause. For each material, three repeats are made at each pre-shear normal stress, and the average results are reported with the error bars indicating the standard deviation of the measurement.

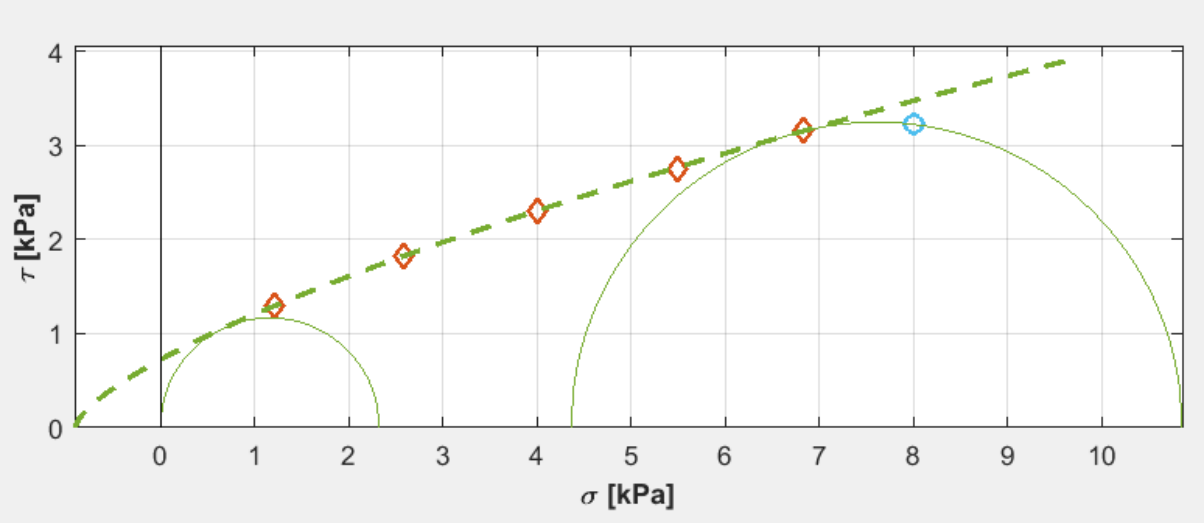

Fig. 7. Yield locus generated using the Warren Spring model at σ_{pre} = 8 kPa.

Following the determination of σ_1 and σ_c at each pre-shear normal stress, the hardness values for all samples were measured by ball indentation at the major principal stresses derived from the FT4 shear cell tests, to allow comparison with shear cell measurements and the constraint factor to be computed using the approach outlined in the introduction. Additionally, indentation tests are conducted at low consolidation stresses, namely 0.1, 0.2, 0.4, 0.6, 0.8 and 1 kPa. For the ball indentation experiments, the criteria for sample, die and indenter dimensions established by Zafar *et al.* [27] are adhered to for this work. A 20 mm diameter stainless steel die, which is attached to a metal plate extending beyond the outer wall of the die, is filled by passing the powder through a sieve with an aperture approximately five times greater than d_{50}. The sieve is placed directly above a funnel, above the die. The die height is 20 mm, with a bed height of 15 - 20 mm generated in all cases, and the powder mass is weighed. The die is placed below a stainless steel piston of 19.8 mm diameter attached to an Instron 1175 mechanical testing machine (Instron, USA) by a 1 N load cell, which has a resolution of 0.25 mN. Before each test is started, the metal plate to which the die is attached is driven towards the piston while the force is recorded (with the die offset to prevent contact with the die walls) until contact is made, in order to determine the distance between the base of the die and the piston. After that, the plate is returned to its starting position, and the die is

centred below the piston. At the start of the actual test, the die is driven upwards, towards the piston, at a vertical speed of 1 mm/min, therefore testing in the quasi-static regime, until the desired consolidation stress is reached. The final displacement of consolidation, z_f, is recorded and used along with the distance between the base of the die and the piston at the starting point, z_o, to determine the bed height, and consequently determine the packing fraction, χ, using Eq. (4):

$$\chi = \frac{\rho_b}{\rho_t} = \frac{M/V}{\rho_t} = \frac{\frac{4M}{\pi(z_0 - z_f)D_d^2}}{\rho_t} \quad (4)$$

where ρ_b and ρ_t are the bulk and true densities, respectively, M and V are the mass and volume of the powder, respectively, and D_d is the die diameter.

The sample is then unloaded at the same velocity, and the piston is replaced by a 4 mm diameter, spherical, stainless steel indenter aligned centrally above the powder bed. The die is then driven upwards, towards the indenter, at the same speed as the consolidation step, until contact is detected, which is considered to be when a force of 3 mN is registered. Following that, the penetration is continued until the desired penetration depth is reached, and the sample is then unloaded. The ball indentation setup is shown in Fig. 8.

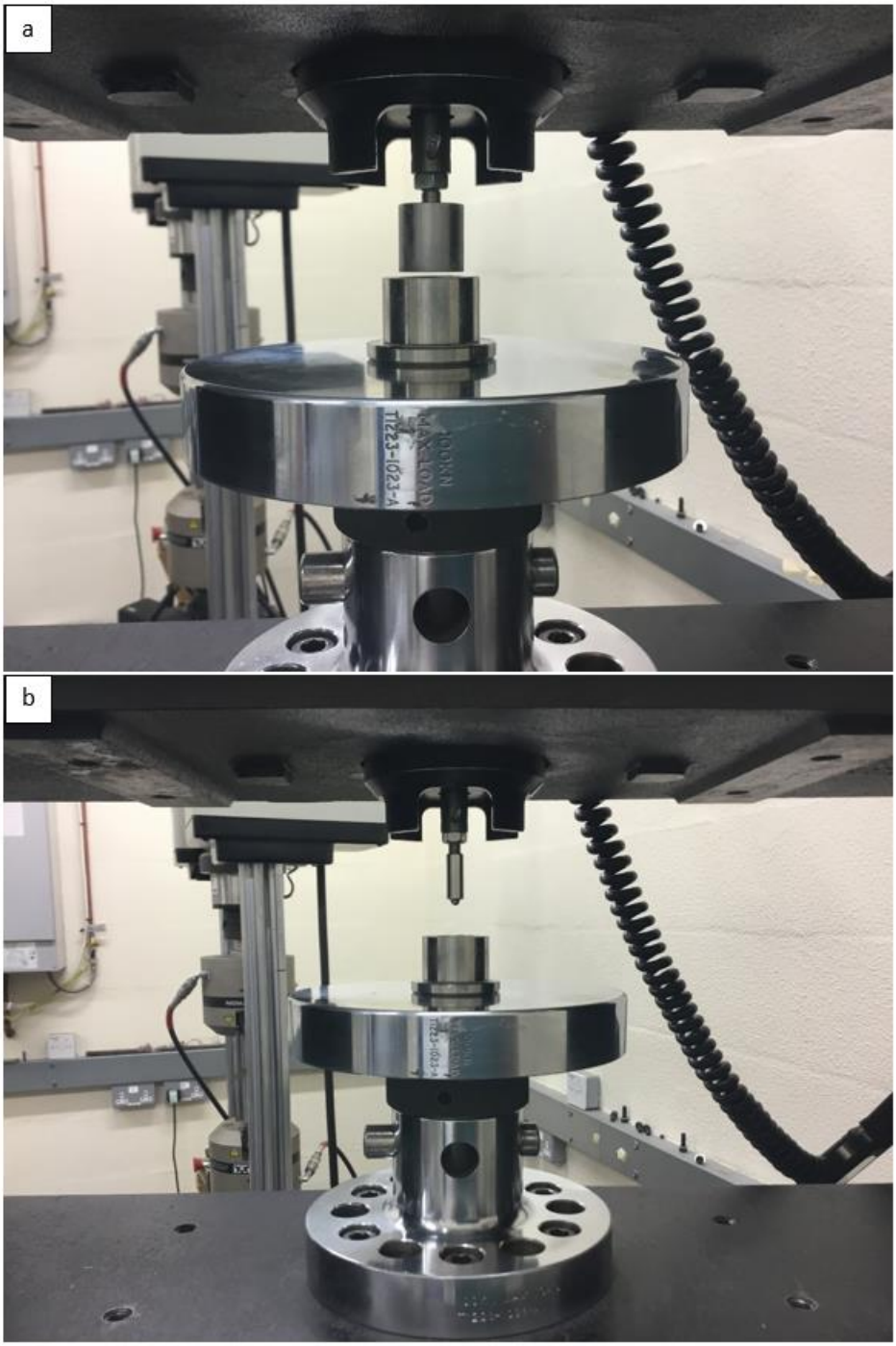

Fig. 8. Ball indentation setup (a: consolidation, b: penetration).

The bed hardness is calculated using Eq. (1), with the projected area of the impression of the indenter determined using Eq. (2). Hardness is typically overestimated at shallow depths, whilst at large penetration depths further consolidation may occur, which also leads to an overestimation of hardness. It is necessary for the measured hardness to be independent of the penetration depth in

order to represent plastic yield stress [32]. The range of penetration depths that provide a stable hardness measurement is therefore determined. The dimensionless penetration depth, h_d, is determined using Eq. (5), with values in the range of 0.1 - 0.7 being applied for each powder at consolidation stresses of 0.1 and 1 kPa.

$$h_d = 2h_c/d_b \quad (5)$$

As such, a dimensionless penetration depth determined to be in the stable hardness range is then applied in all experiments for the remaining consolidation stresses for a given powder. The ball indentation technique is applied at the major principal stresses determined in the shear cell experiments, where it is assumed that the normal stress in the indentation process is equal to the major principal stress. The constraint factor is then determined at these major principal stresses. In addition, the ball indentation method is applied at low consolidation stresses of 0.1, 0.2, 0.4, 0.6, 0.8 and 1 kPa. The unconfined yield strength is then inferred at these stresses using Eq. (3) and the established constraint factor for the powder. For each material, five repeats are made at each pre-shear normal stress, and the average results are reported with the error bars indicating the standard deviation of the measurement. For all the experiments carried out here the temperature was 20 - 25 ^{o}C and the relative humidity (RH) was 30 - 65 %.

3 Results and discussion

3.1 Effect of particle size on constraint factor and flow behaviour

The measurements of unconfined yield strength at the corresponding major principal stresses determined for five consecutive single sieve cuts of glass beads silanised by Sigmacote® are shown in Table 2. For all sizes, the unconfined yield strength is found to increase approximately linearly with major principal stress, whilst decreasing with increasing particle size, as shown in Fig. 9. For a given pre-shear normal stress, there is a clear increase in flowability with increasing particle size, as evidenced from the ff_c values in Table 2. In addition to this, the flow function coefficient increases

with pre-shear normal stress, and ranges from 1.6 - 4.2 for the 45 - 53 µm glass beads to 2.4 - 6.3 for the 90 - 106 µm glass beads.

Table 2. FT4 shear test data for five consecutive single sieve cuts of silanised glass beads.

	45 - 53 µm			53 - 63 µm			63 - 75 µm			75 - 90 µm			90 - 106 µm		
σ_{pre}	σ_1	σ_c	ff_c	σ_1	σ_c	ff_c	σ_1	σ_c	ff_c	σ_1	σ_c	ff_c	σ_1	σ_c	ff_c
2	3.2	2.0	1.6	3.2	1.8	1.8	3.1	1.5	2.1	3.1	1.5	2.1	3.0	1.3	2.4
4	5.7	2.2	2.6	5.8	2.0	2.9	5.7	1.8	3.1	5.7	1.6	3.7	5.7	1.5	3.8
6	8.2	2.3	3.5	8.3	2.1	3.9	8.3	1.9	4.3	8.4	1.8	4.6	8.3	1.7	5.0
8	10.8	2.6	4.2	10.9	2.4	4.6	10.9	2.1	5.2	10.9	1.9	5.9	10.8	1.7	6.3

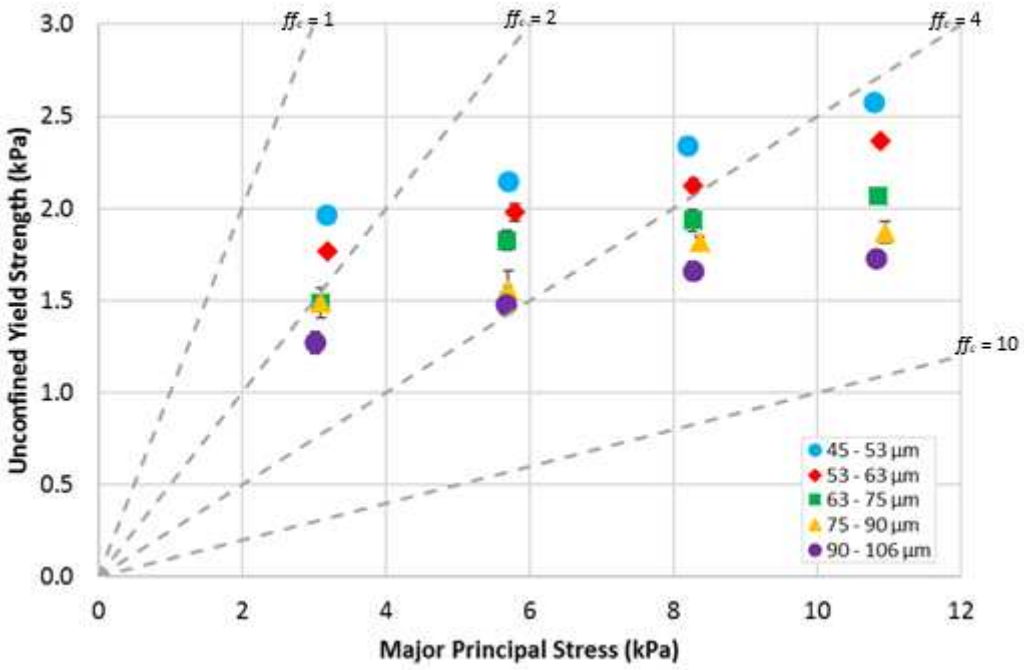

Fig. 9. Unconfined yield strength as a function of major principal stress for five consecutive single sieve cuts of silanised glass beads.

Hardness measurements at dimensionless penetration depths of 0.1, 0.3, 0.5 and 0.7 were performed on separate powder beds of 63 - 75 µm glass beads consolidated to 0.1 and 1 kPa, as shown in Fig. 10. The dimensionless penetration depths are calculated using Eq. (5). It can be seen that for both tested consolidation stresses hardness is overestimated at a dimensionless penetration depth of 0.1. This phenomenon is observed for all materials at shallow indentation depths. However,

beyond this point hardness reaches a plateau, becoming constant for dimensionless penetration depths greater than 0.3.

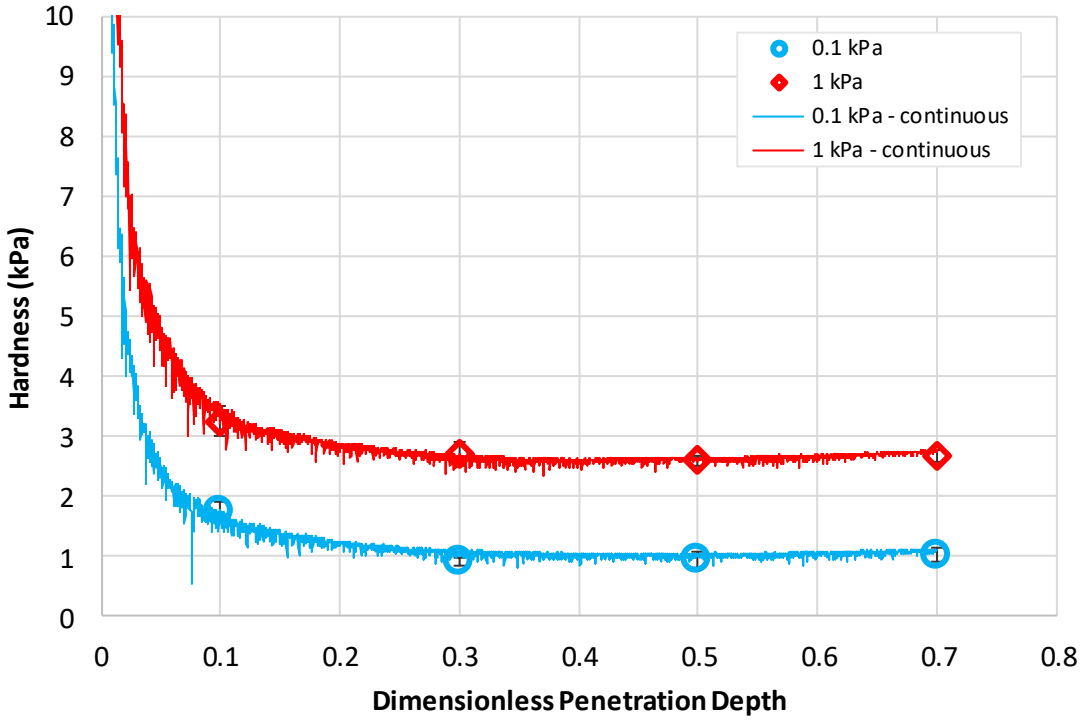

Fig. 10. Hardness as a function of dimensionless penetration depth for the 63 - 75 µm single sieve cut of silanised glass beads.

These findings are in agreement with the DEM simulations of Pasha *et al.* [28] and the experiments of Zafar *et al.* [27]. Here the hardness was determined by considering the penetration depth at maximum indentation load rather than the elastically-recovered depth. Fig. 11 shows the force-displacement profile for indentation up to a dimensionless penetration depth of 0.5 for a bed of 63 - 75 µm glass beads consolidated to 10.9 kPa. The hardness calculated at the highest major principal stress of 10.9 kPa for the 63 - 75 µm sample, by considering the projected area of the impression of the indenter after unloading, was found to be almost identical (< 0.2 % difference) to the value computed by using the penetration depth at maximum indentation load to determine hardness, i.e. by ignoring unloading. This is expected given the almost vertical slope of the unloading curve. If the

unloading effect is ignored, then hardness can be estimated at any penetration depth up to the depth tested. In Fig. 10 this is referred to as 'continuous hardness', and is calculated from indentation tests at a dimensionless penetration depth of 0.7. This estimate is shown to be almost identical to the direct measurement made at lower depths for both stresses, since the unloading is negligible for this material. The effect of unloading on hardness was also investigated at the highest major principal stresses for all other samples of glass beads tested in this work, and was found to be negligible. As a result, the use of the penetration depth at maximum indentation load in hardness calculations is justified for this material, it was therefore considered for all the hardness calculations. Furthermore, the behaviour of hardness as a function of penetration depth is independent of the applied stress, therefore the obtained trends at higher stresses are expected to be qualitatively the same, with the same depth range providing valid measurements. This behaviour is consistent for all other sizes of glass beads investigated in this work. With the reliable range of hardness measurements now established, a dimensionless penetration depth of 0.5 is applied for all following ball indentation measurements on silanised glass beads.

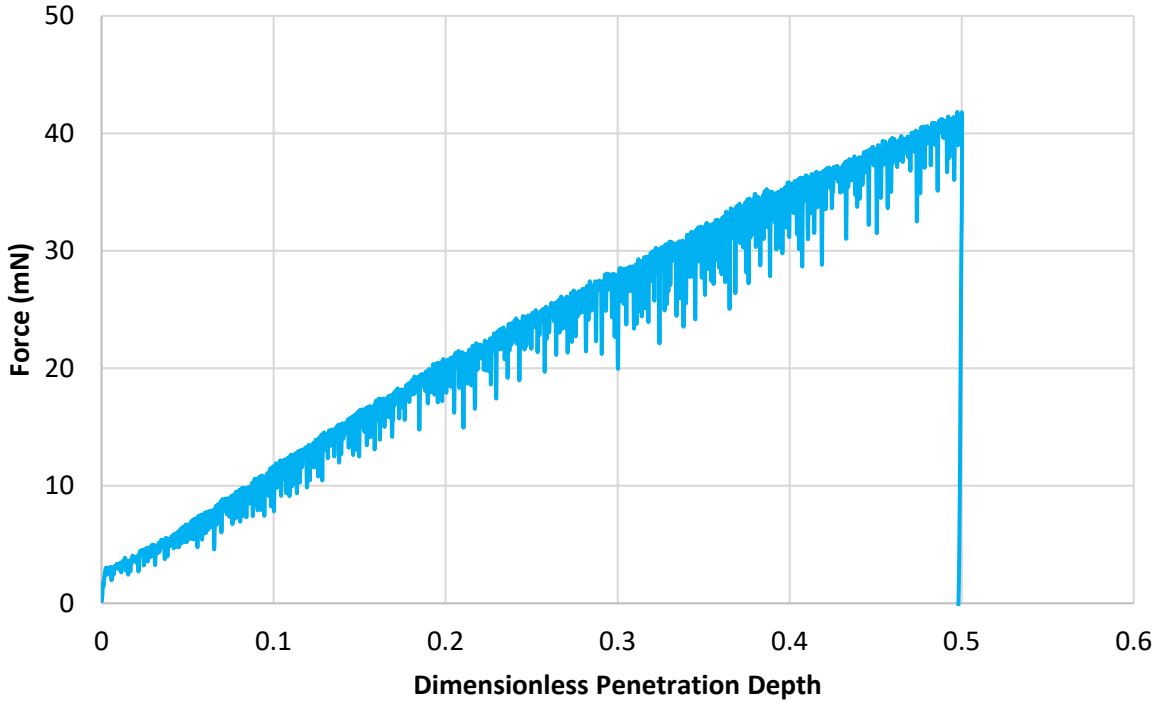

Fig. 11. Force as a function of dimensionless penetration depth during indentation of a 63 - 75 µm glass beads bed at 10.9 kPa.

Although a 3 mN force is taken to indicate contact between the indenter and the powder bed, the indenter penetrates the specimen slightly before this target force is reached. This can be seen from the slope of the force-displacement curve during the contact detection step in Fig. 12. The penetration depth is controlled from the point that the 3 mN force is detected, however the actual penetration depth is determined based on the point contact is made. Consequently, even though the target dimensionless penetration depth for all hardness measurements was 0.5, the true dimensionless penetration depth was larger and varied between tests. However, this does not affect the validity of most of the hardness measurements (particularly at moderate to high stresses), since the true dimensionless penetration depth of 0.7 was not exceeded, and the measurements have already been shown to be independent of penetration depth for dimensionless penetration depths of 0.3 - 0.7. In some repeats at very low stresses though, the dimensionless penetration depth of 0.7

353 was exceeded, and hardness was overestimated, however in most cases this overestimation was
354 within test error.

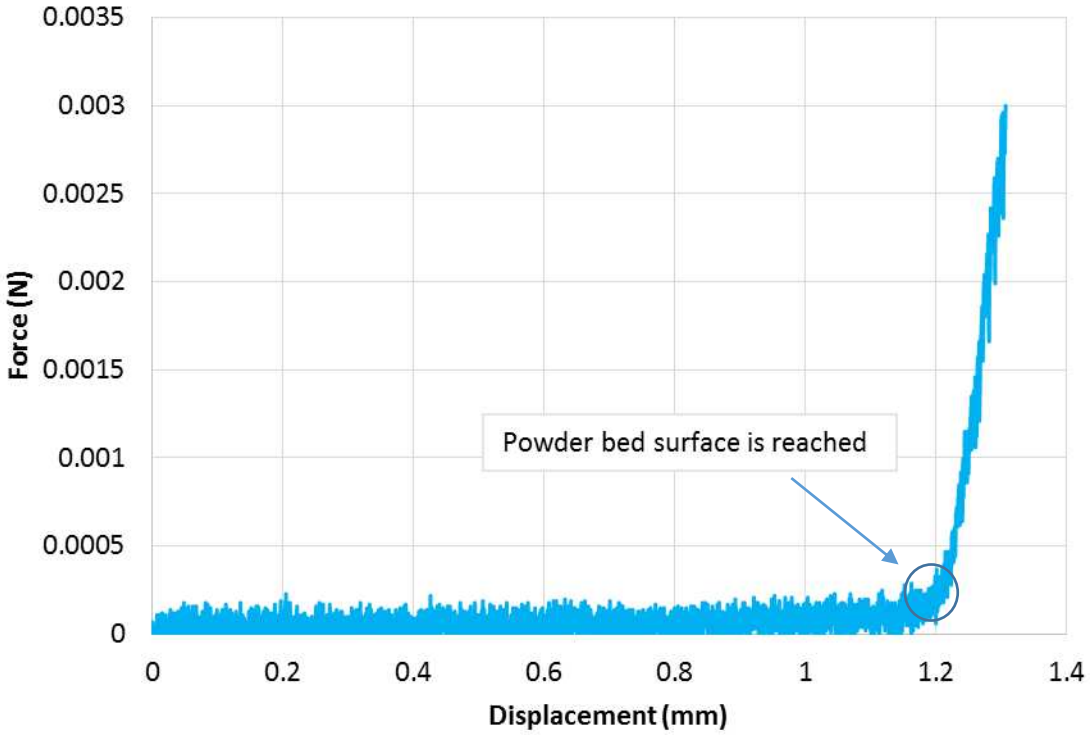

355
356

357 **Fig. 12.** Force against displacement during indentation of a 63 - 75 µm glass beads bed.

358

359 The ball indentation method is applied for all five consecutive single sieve cuts of silanised glass
360 beads using the average major principal stress determined from the three shear cell tests for each
361 sample at each pre-shear normal stress, with the results presented in Fig. 13. At high stresses (> 1
362 kPa) the hardness values of the five sieve cuts are distinctively different, following the same trend as
363 the shear cell results; increasing approximately linearly with major principal stress, and decreasing
364 with an increase in particle size. At low stresses (≤ 1 kPa) the increase of hardness with stress is
365 observed to be much steeper than at high stresses, a phenomenon also observed by Zafar [32].
366 Furthermore, in the case of weakly consolidated powder beds, hardness values are not distinctively
367 different among the different particle sizes. In this range the error bars are somewhat larger, due to
368 the difficulty of reproducing a uniformly flat powder bed surface, as well as creating a consistent

packing structure. As the applied consolidation stress increases, the influence of bed surface asperities becomes less important. At all stress levels the standard deviation of five measurements (indicated by the error bars) is low; with the coefficient of variation being less than 10 % in most cases.

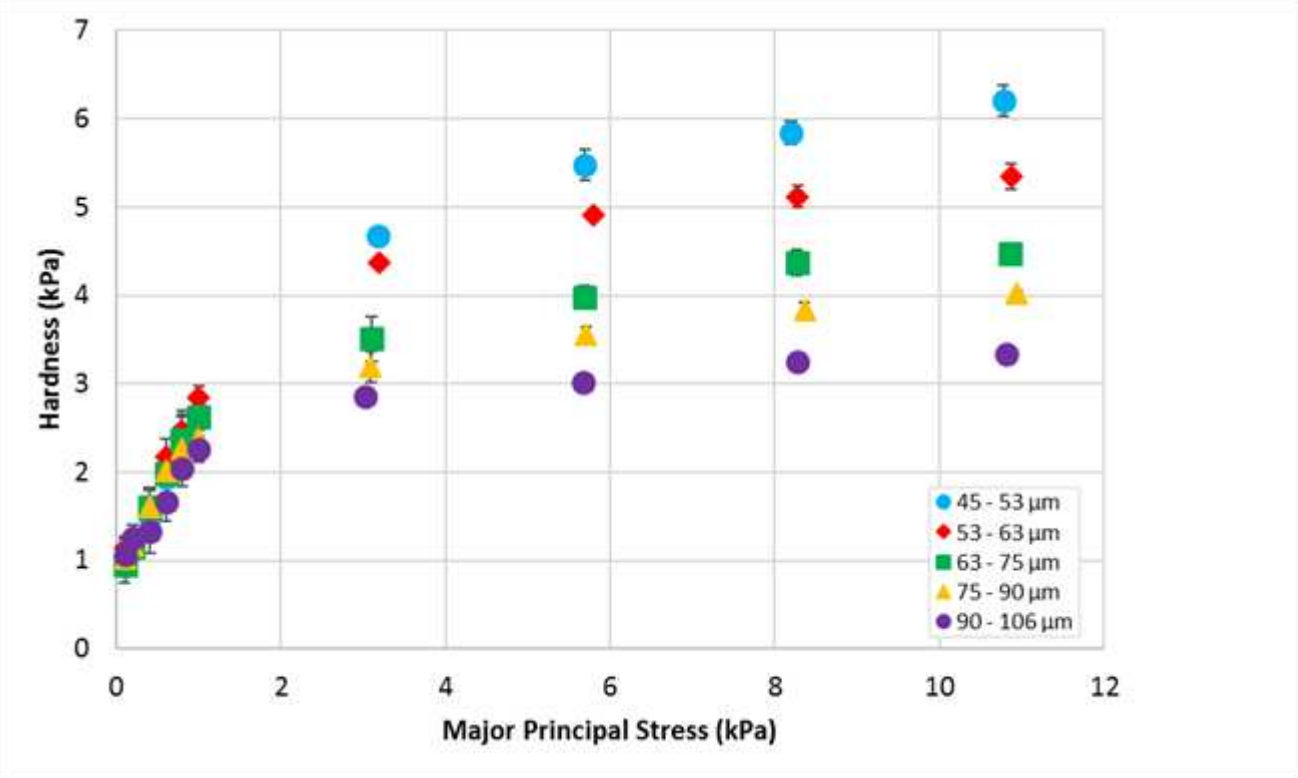

Fig. 13. Hardness as a function of major principal stress for five consecutive single sieve cuts of silanised glass beads.

In order to investigate the cause of the discrepancy of the hardness increase against stress between high and low stresses, the packing fraction for all five sieve cuts is calculated using Eq. (4), and is shown against major principal stress in Fig. 14.

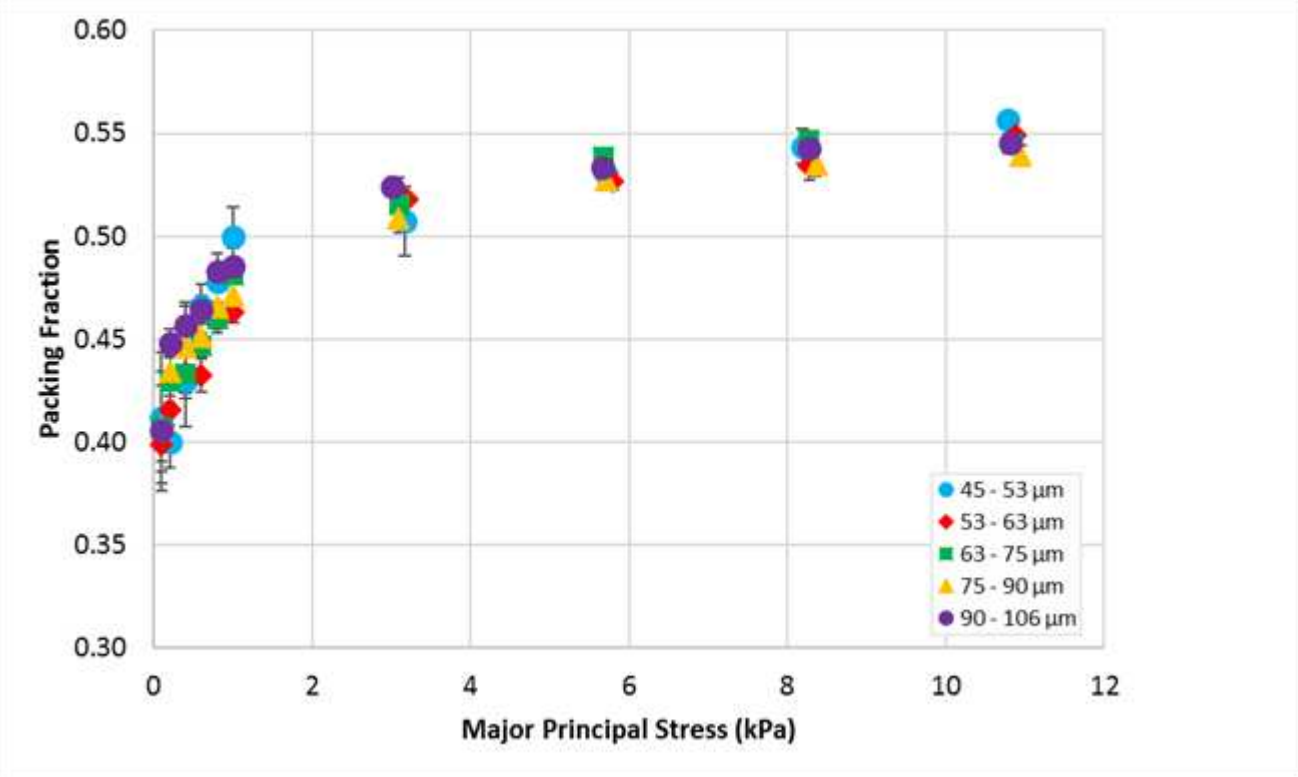

Fig. 14. Packing fraction against major principal stress for five consecutive single sieve cuts of silanised glass beads.

As can be seen from Fig. 14, all glass bead samples exhibit a dramatic increase of packing fraction with the increase of consolidation stress in the low stress region. A small increase of the applied stress leads to a much more compacted powder bed, which in turn provides a great increase of resistance to plastic deformation. On the other hand, in the high stress region, the packing state of the powder beds does not change considerably with the applied stress. The aforementioned behaviour leads to an approximately linear increase of hardness with packing fraction in the range 0.45 - 0.55, as shown in Fig. 15. Generally hardness is greater for smaller particles at a given packing fraction, although this behaviour is clear only at high stresses. At low stresses the error bars of packing fraction are significant, and the difference in hardness among the different particle sizes is not clear.

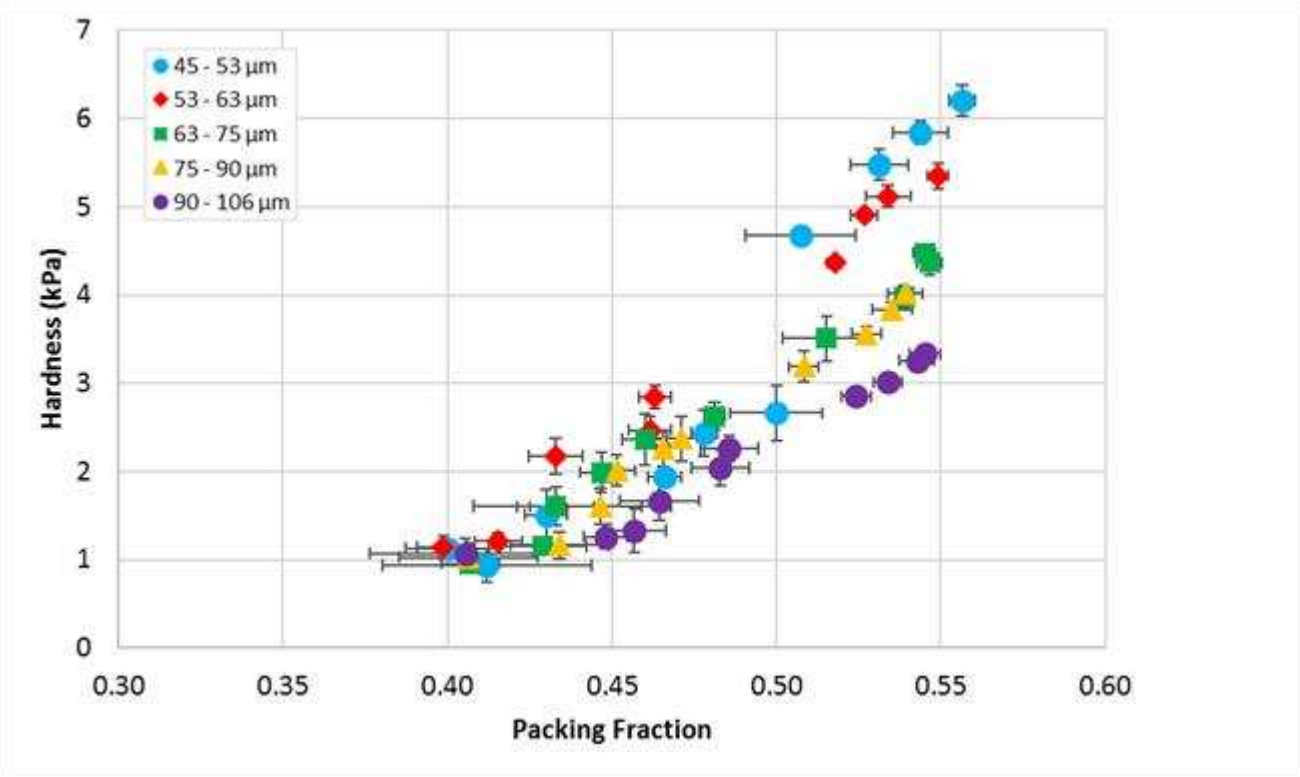

394

395 **Fig. 15.** Hardness as a function of packing fraction for five consecutive single sieve cuts of silanised
396 glass beads.
397

398 The constraint factor is determined at each stress level for all sieve cuts of silanised glass beads using
399 Eq. (3) and the measurements of unconfined yield strength and hardness, and presented against
400 major principal stress in Fig. 16. The constraint factor is shown to be approximately constant for a
401 given sieve cut across all tested major principal stresses. Moreover, *C* is found to generally decrease
402 with an increase in particle size. These findings agree with the work of Zafar [32].

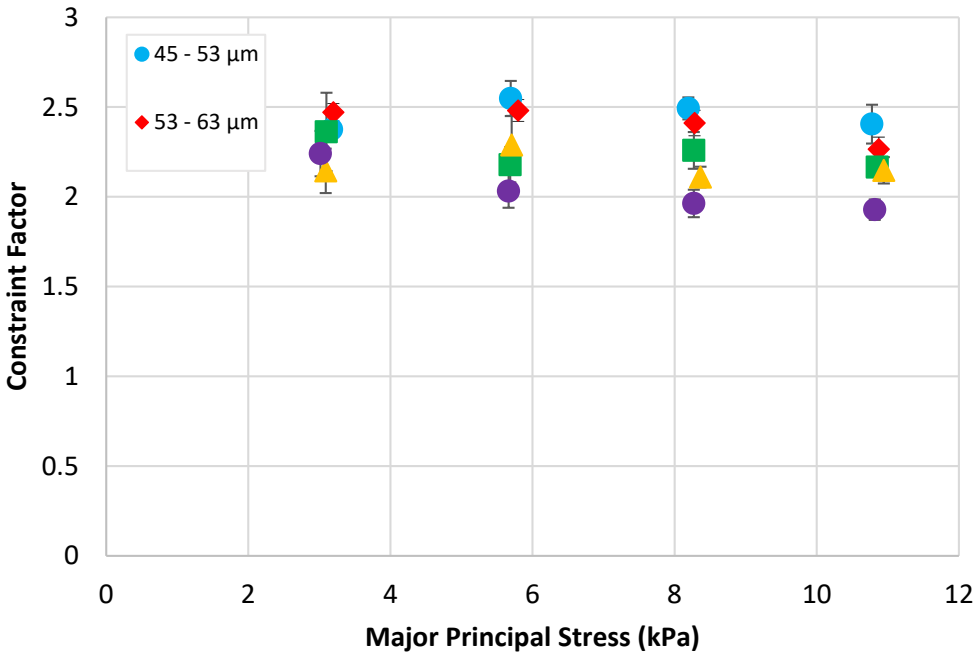

403
404

405 **Fig. 16.** Constraint factor as a function of major principal stress for five consecutive single sieve cuts
406 of silanised glass beads.

407

408 Since the constraint factor was found to be virtually independent of the major principal stress
409 applied, it is assumed to remain constant at low stresses. This assumption is validated by DEM
410 simulations of Stavrou *et al.* [29], which show *C* to remain constant down to the lowest investigated
411 stress of 0.1 kPa. For all samples, the average constraint factor across all major principal stresses is
412 used along with the ball indentation measurements at low consolidation stresses to determine the
413 unconfined yield strength at such stresses via Eq. (3). Fig. 17 shows the inferred unconfined yield
414 strength values from the ball indentation measurements at major principal stresses of 0.1, 0.2, 0.4,
415 0.6, 0.8 and 1.0 kPa, along with the unconfined yield strength measurements carried out in the shear
416 cell at pre-shear normal stresses of 2, 4, 6 and 8 kPa shown in Fig. 9. The indentation technique
417 suggests a significant reduction in unconfined yield strength at lower consolidation levels in
418 comparison to values that would be linearly extrapolated from the shear tests.

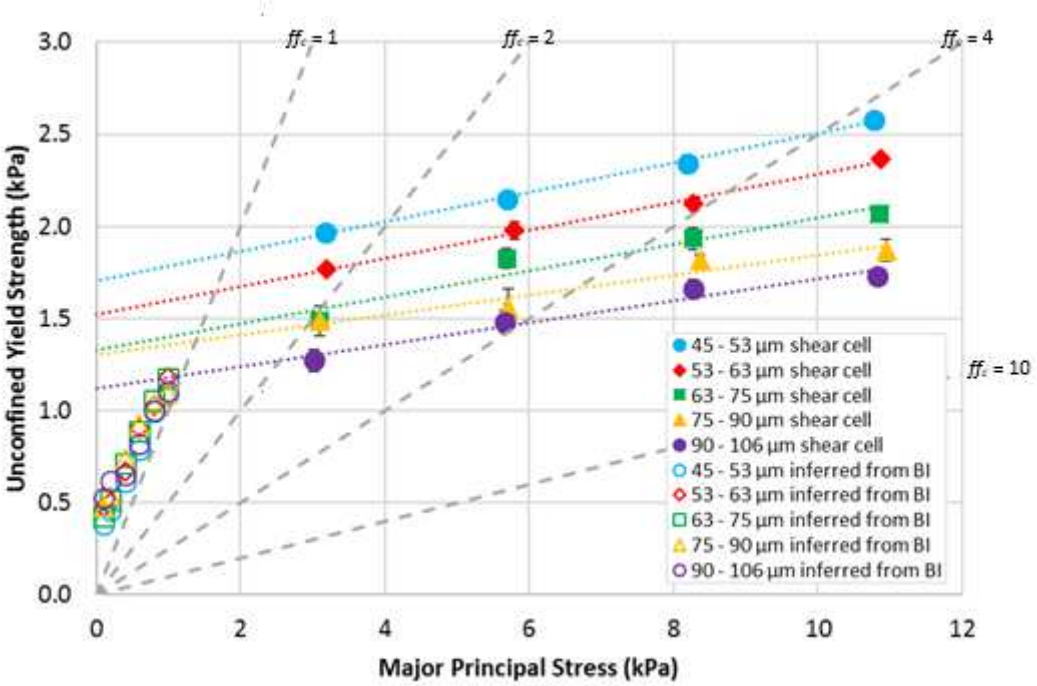

Fig. 17. Unconfined yield strength shear cell measurements and inferred values from ball indentation for five consecutive single sieve cuts of silanised glass beads.

Measurement of unconfined yield strength at low stresses is often not reliable, or even possible, using a shear cell, however the shear cell is more likely to achieve steady-state failure, and therefore generate a result, for more cohesive powders. Since the 45 - 53 µm are the most cohesive glass beads used here, shear cell measurements are made at pre-shear normal stresses of 0.06, 0.1, 0.25, 0.5 and 1 kPa for this sample, and are shown compared to the indentation measurements in Fig. 18. The trends of unconfined yield strength against major principal stress are remarkably similar in this low stress range for both techniques.

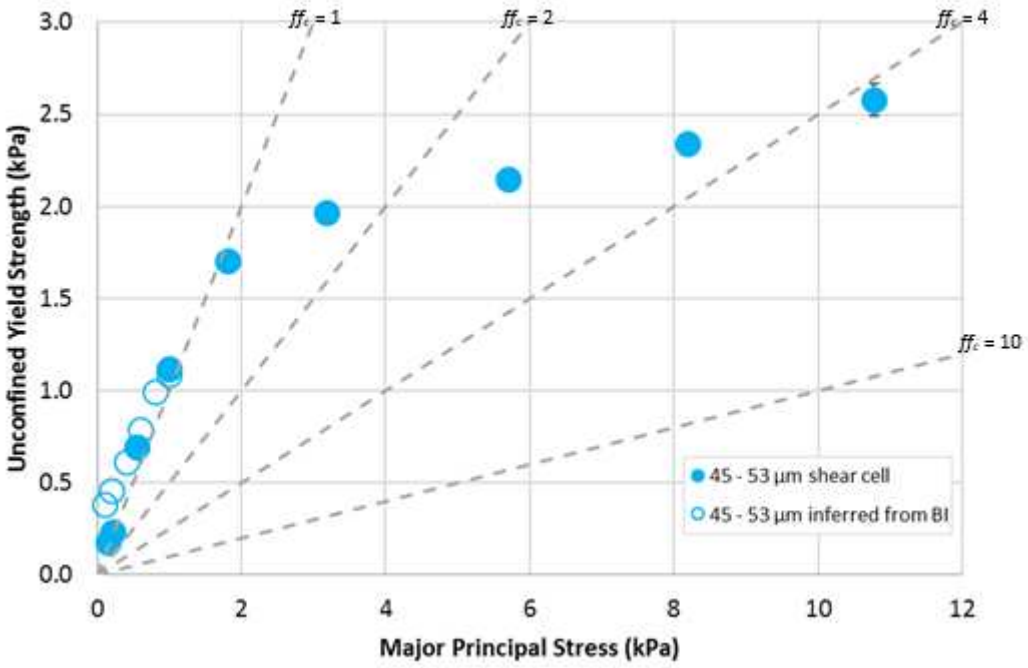

430

431 **Fig. 18.** Unconfined yield strength at low stresses determined from the shear cell and ball
432 indentation for the 45 - 53 µm single sieve cut of silanised glass beads.
433

434 In order to further investigate the shear cell measurements, the measured shear stresses and
435 applied normal stresses of three repeats of the FT4 shear cell measurements at the pre-shear normal
436 stresses of 0.06, 0.25, 1, 4, and 8 kPa, are shown in Fig. 19. At pre-shear normal stresses of 0.06 and
437 0.25 kPa the data show great variation among repeats, with the generated yield loci not consistently
438 showing a monotonic increase in shear stress with normal stress. In addition to this, in both cases
439 there is notable discrepancy between the target normal stresses and the actual applied stresses. The
440 nature of the FT4 shear cell protocol, which leads to shearing from the highest to the lowest chosen
441 target stress, can lead to data points for which the shear stress exceeds the pre-shear stress when
442 the applied stress is greater than the target stress, which invalidates the measurement. This
443 phenomenon is observed in the case of tests at 0.06 kPa, where stresses beyond 0.06 kPa have been
444 applied during the shear test, and leads to an overestimation of the unconfined yield strength,
445 however this is not observed at higher stresses. At a pre-shear normal stress of 1 kPa the generated

446 test data are highly reproducible, although the applied stresses are still not equidistant, and deviate
447 notably from the target normal stresses, but less so than at lower pre-shear normal stresses. At a
448 pre-shear normal stress of 4 kPa, the shear tests are highly reproducible and the achieved stresses
449 are equidistant, though deviate slightly from the target normal stresses. At 8 kPa, not only are the
450 tests highly reproducible, but the target stresses have been virtually achieved. Therefore, a general
451 trend of increasing reliability and reproducibility of shear testing is observed as the pre-shear normal
452 stress is increased. This highlights the need for detailed analysis of shear cell data to assess the
453 validity of the measured yield locus, particularly at low pre-shear normal stresses.

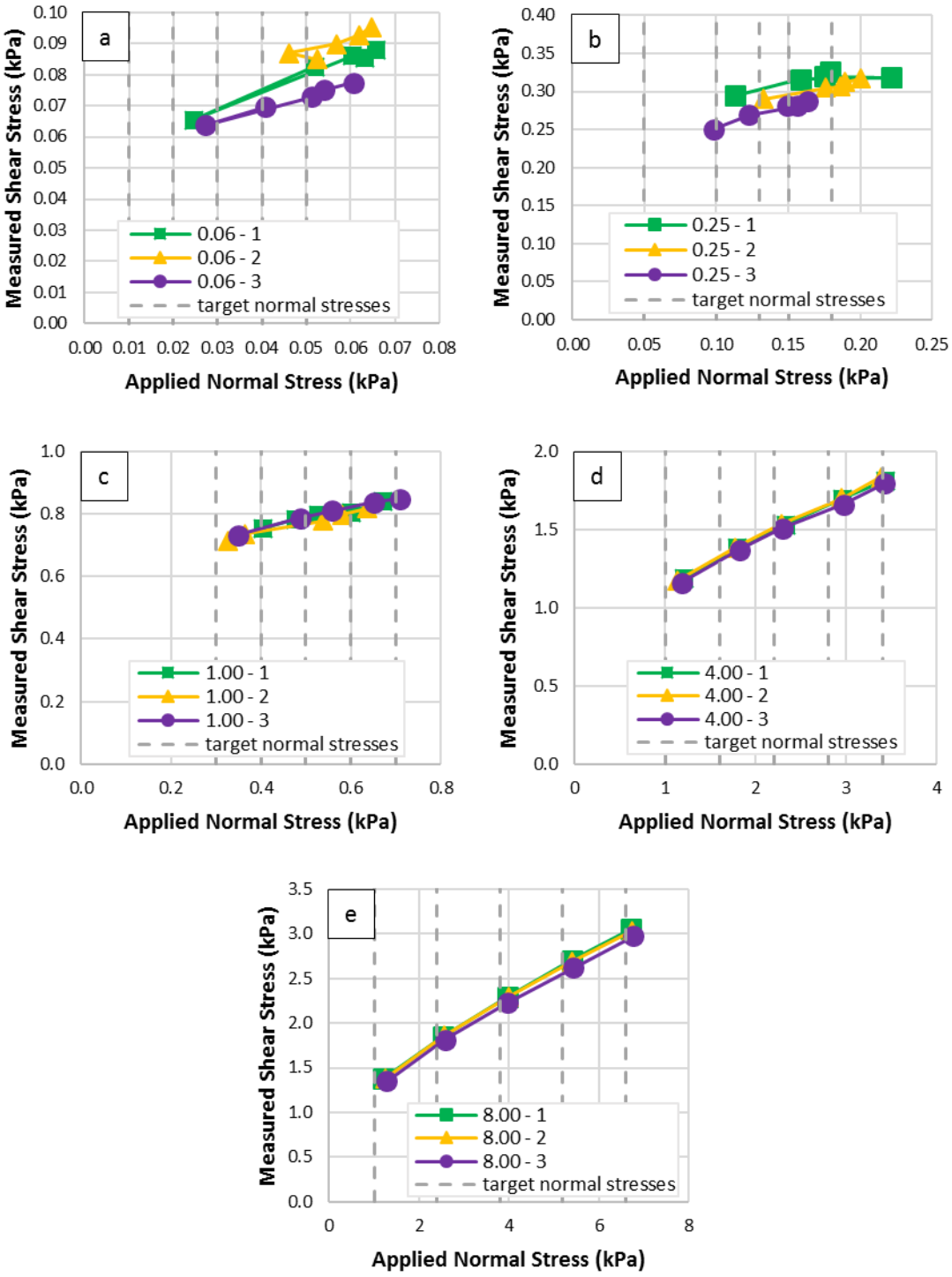

Fig. 19. Measured shear and applied normal stresses for 45 - 53 µm silanised glass beads at pre-shear normal stresses of a) 0.06 kPa, b) 0.25 kPa, c) 1.00 kPa, d) 4.00 kPa and e) 8.00 kPa.

3.2 Flowability of silanised glass bead mixtures of varying particle size distribution

3.2.1 Effect of width of particle size distribution on constraint factor and flow behaviour

The FT4 shear cell measurements of unconfined yield strength at the corresponding major principal stresses are shown in Table 3 for the medium 63 - 75 µm single sieve cut, along with two mixtures of 53 - 90 µm and 45 - 106 µm of silanised glass beads. The two mixtures have essentially the same d_{50} as the single sieve cut, but wider size distributions, as reported in Table 1. As the size distribution is widened, the d_{10} and d_{90} reduce and increase, respectively, by about 3 - 4 µm with each additional sieve cut. The unconfined yield strength against major principal stress is shown in Fig. 20. Unconfined yield strength increases approximately linearly with major principal stress, as with the single sieve cuts in section 3.1. It can be seen from both Table 3 and Fig. 20 that at a given pre-shear normal stress there is a slight increase in unconfined yield strength as the size distribution is widened. Moreover, ff_c is found to increase with the pre-shear normal stress applied and decrease as the size distribution is widened.

Table 3. FT4 shear test data for three samples of silanised glass beads with varying width of size distribution.

	63 - 75 µm			**53 - 90 µm**			**45 - 106 µm**		
σ_{pre}	σ_1	σ_c	ff_c	σ_1	σ_c	ff_c	σ_1	σ_c	ff_c
2	3.1	1.5	2.1	3.2	1.6	1.9	3.2	1.8	1.8
4	5.7	1.8	3.1	5.8	1.9	3.1	5.8	2.0	2.9
6	8.3	1.9	4.3	8.4	2.1	4.1	8.4	2.2	3.8
8	10.9	2.1	5.2	10.9	2.2	5.0	11.0	2.4	4.6

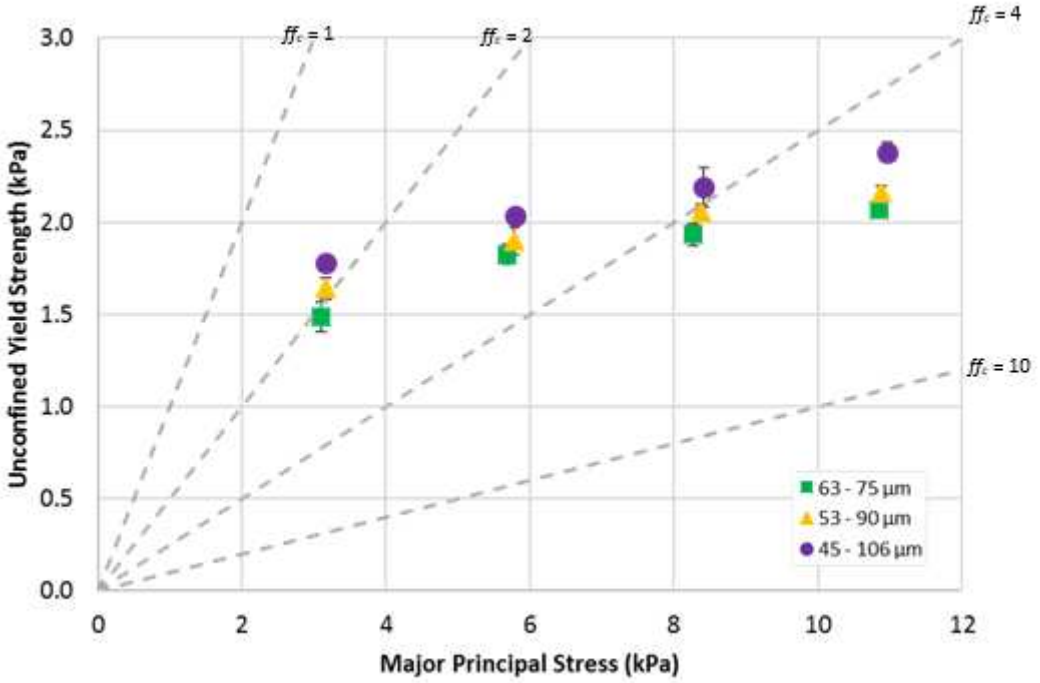

Fig. 20. Unconfined yield strength as a function of major principal stress for three samples of silanised glass beads with varying width of size distribution.

Fig. 21 shows the hardness measurements made at all major principal stresses for all three size distributions of silanised glass beads. As with the unconfined yield strength from the shear tests above, hardness is observed to marginally increase when widening the size distribution at higher stresses, whereas no notable difference can be seen at low stresses. As with Fig. 13, indentation tests indicate a more rapid increase of hardness with major principal stress for weakly consolidated powder beds, which is explained by the packing fraction trend presented in Fig. 22.

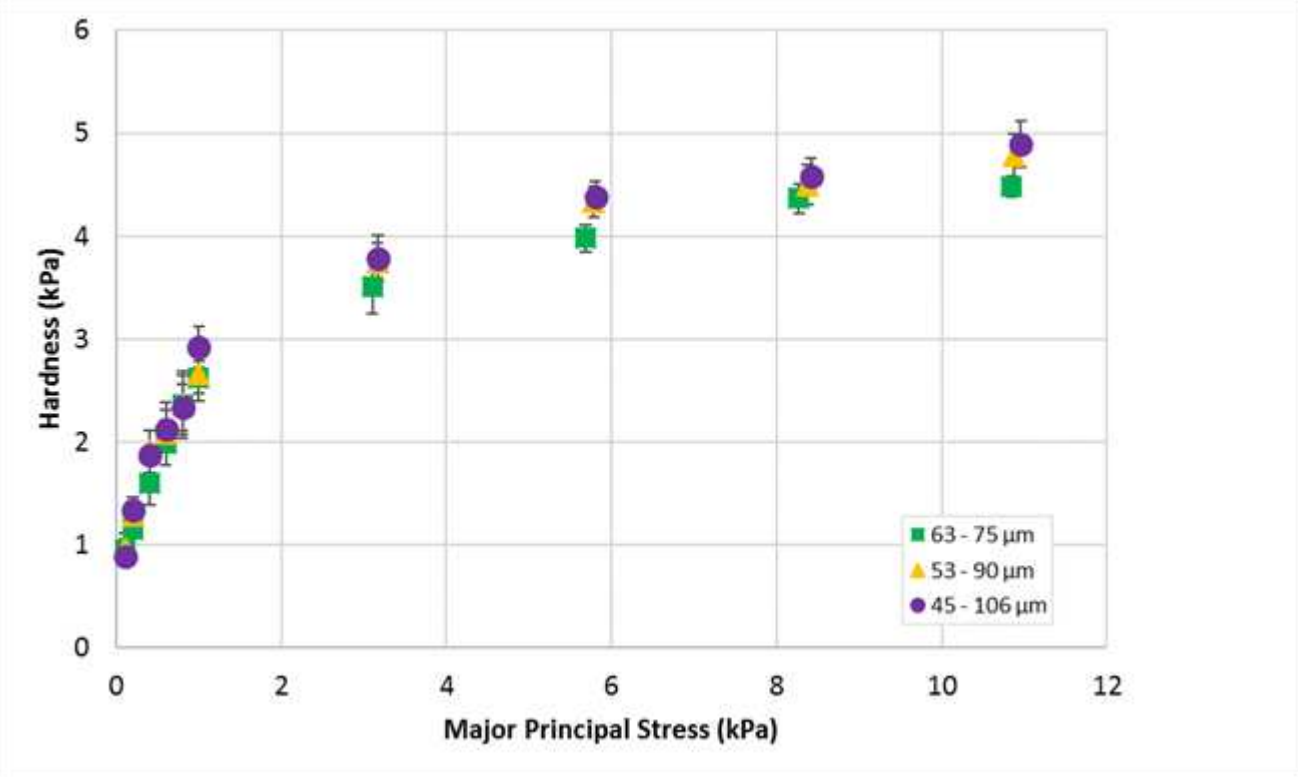

Fig. 21. Hardness as a function of major principal stress for three samples of silanised glass beads with varying width of size distribution.

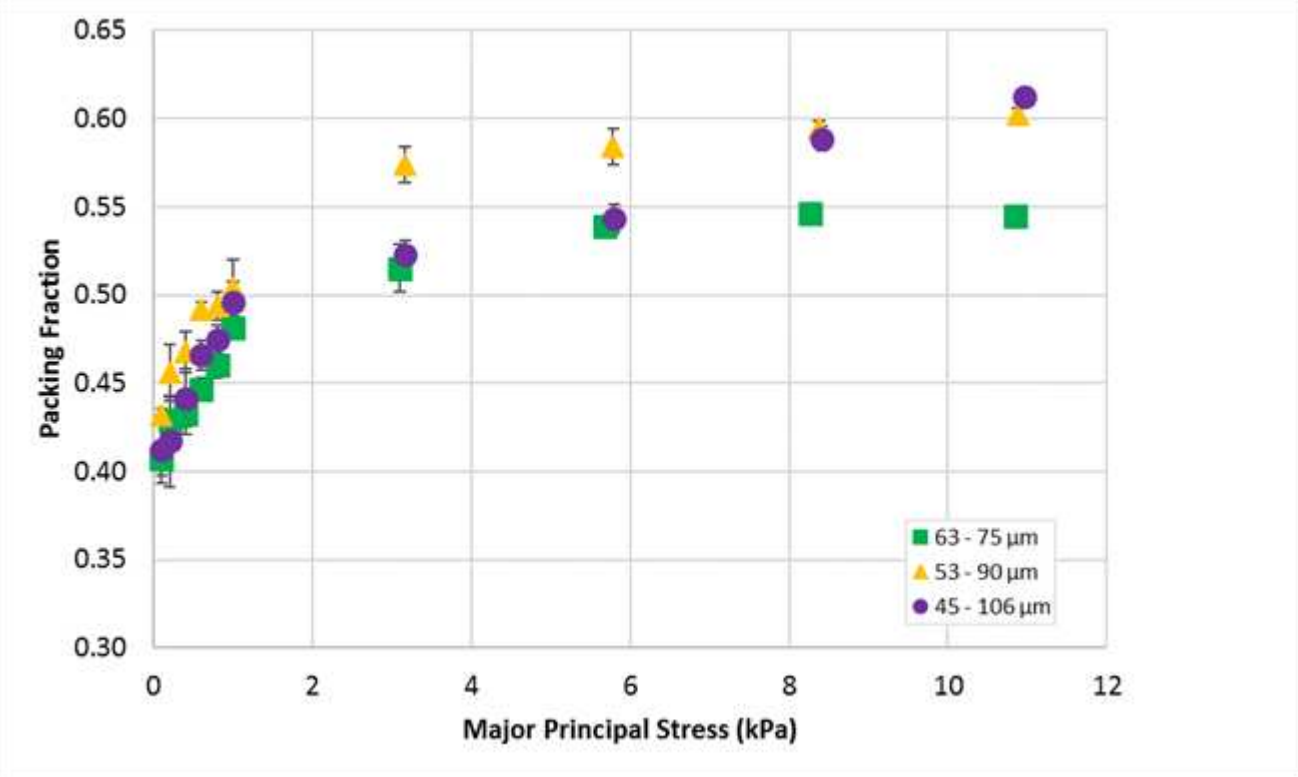

492

493 **Fig. 22.** Packing fraction as a function of major principal stress for three samples of silanised glass
494 beads with varying width of size distribution.

495

496 The constraint factor determined from the ball indentation and shear cell measurements for all size
497 distributions is shown in Fig. 23. Once again, constraint factor is found to remain constant
498 throughout the range of consolidation stresses applied. In addition to this, a slight reduction in
499 constraint factor is observed with an increase in the span of the sample, however this effect may not
500 be statistically significant.

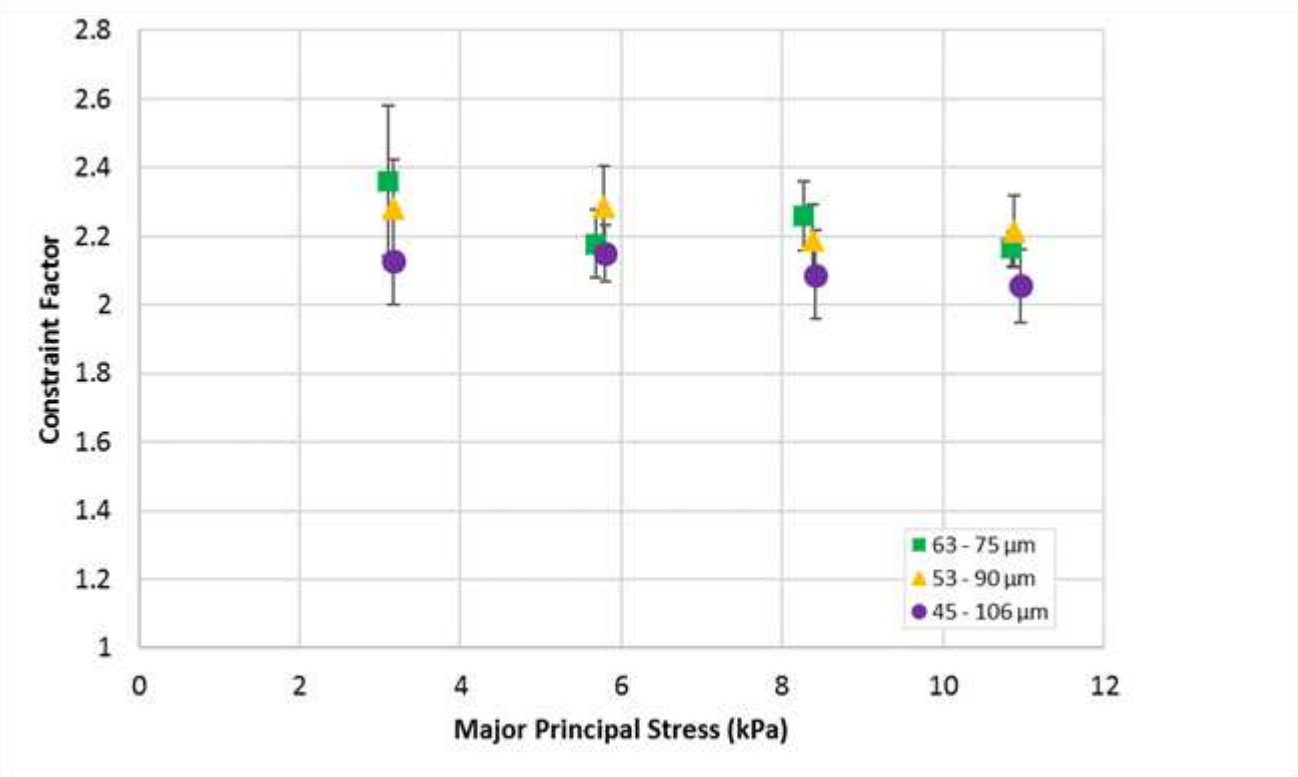

Fig. 23. Constraint factor as a function of major principal stress for three samples of silanised glass beads with varying width of size distribution.

Fig. 24 shows the unconfined yield strength values inferred from the ball indentation method at low stresses, along with the measurements made in the shear cell at higher stresses. As in the case of the consecutive single sieve cuts, the increase of the unconfined yield strength is estimated to be sharper with increasing major principal stress at lower stresses. At lower stresses the inferred values of unconfined yield strength are not distinctively different among the samples.

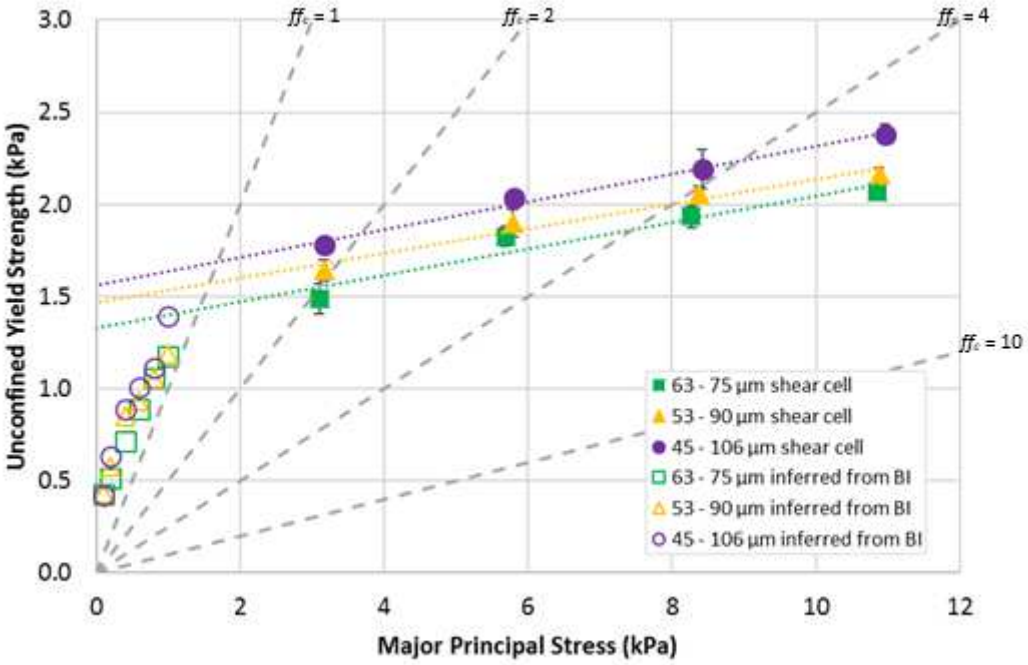

510

511 **Fig. 24.** Unconfined yield strength shear cell measurements and inferred values from ball indentation
512 for three samples of silanised glass beads with varying width of size distribution.

513

514 3.2.2 Effect of d_{10} and d_{90} on constraint factor and flow behaviour

515 The FT4 shear testing data of 63 - 75 µm silanised glass beads mixed with 10 % and 20 % w/w coarse
516 and fine particles are reported in Table 4, along with the data for the 63 - 75 µm single sieve cut for
517 comparative purposes. The unconfined yield strength against major principal stress is shown in Fig.
518 25. The addition of coarse particles is found to have negligible effect on the unconfined yield
519 strength regardless of the quantity added, whilst the addition of fines substantially increases the
520 unconfined yield strength, with a further increase observed as the quantity added increases. This is
521 in agreement with the finding of Molerus and Nwylt [19] that unconfined yield strength increases
522 with fines content up to 30 % w/w, beyond which it becomes equal to the strength of the fines
523 alone. The addition of 20 and 10 % w/w coarse particles can be viewed as 80 and 90 % w/w 63 - 75
524 µm added, respectively, to the 150 - 180 µm sample, and so the yield strength of the mixtures is
525 essentially equal to the yield strength of the 63 - 75 µm sample in this case. Adding 10 % w/w coarse

particles leads in most cases to a slight reduction in ff_c, with an increase in coarse content to 20 % w/w coarse particles causing the flow function coefficient to slightly increase again. The flow function coefficient decreases with the addition of fines, as shown in Table 4.

Table 4. FT4 shear test data for 63 - 75 µm silanised glass beads mixed with varying amounts of coarse and fine particles, along with the 63 - 75 µm single sieve cut.

	63 - 75 µm + 20 % coarse			63 - 75 µm + 10 % coarse			63 - 75 µm			63 - 75 µm + 10 % fines			63 - 75 µm + 20 % fines		
σ_{pre}	σ_1	σ_c	ff_c	σ_1	σ_c	ff_c	σ_1	σ_c	ff_c	σ_1	σ_c	ff_c	σ_1	σ_c	ff_c
2	3.2	1.6	2.0	1.7	1.8	1.9	3.1	1.5	2.1	3.3	2.0	1.7	3.5	2.5	1.4
4	5.8	1.6	3.8	5.9	1.9	3.1	5.7	1.8	3.1	6.2	2.4	2.6	6.5	3.5	1.8
6	8.4	2.0	4.2	8.5	2.1	4.0	8.3	1.9	4.3	8.9	2.4	3.8	9.4	4.4	2.2
8	10.9	2.1	5.1	11.0	2.2	5.0	10.9	2.1	5.2	11.6	2.9	4.0	12.2	4.7	2.6

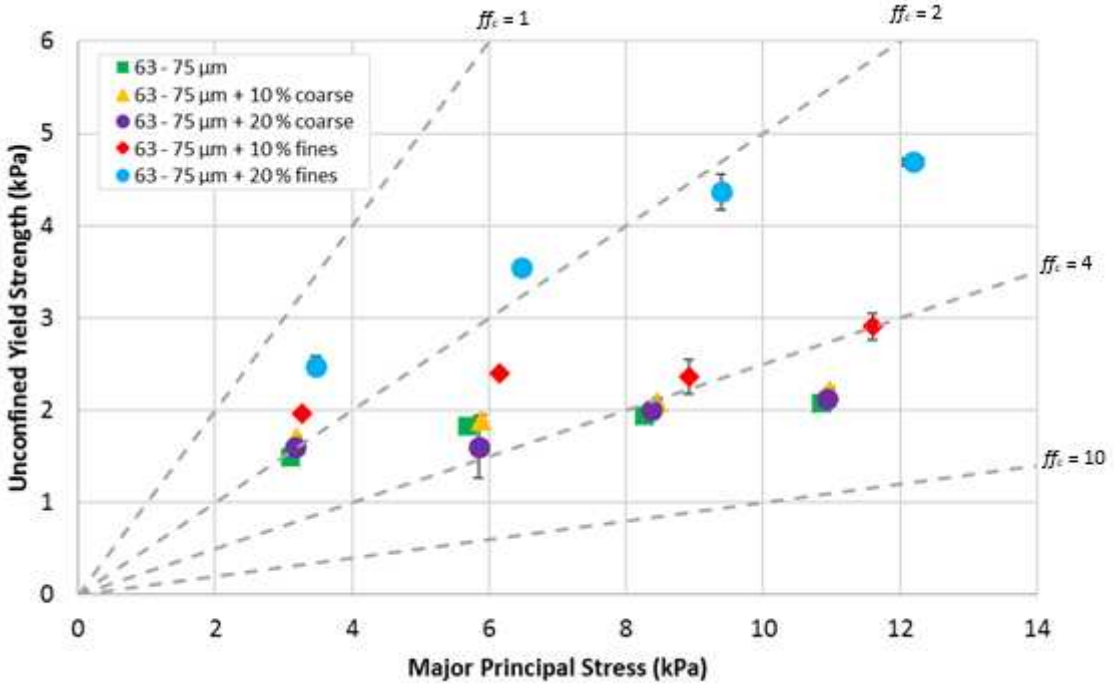

Fig. 25. Unconfined yield strength as a function of major principal stress for 63 - 75 µm silanised glass beads mixed with varying amounts of coarse and fine particles, along with the 63 - 75 µm single sieve cut.

Fig. 26 shows the hardness against major principal stress for the same mixtures of glass beads. A reduction of d_{10} (addition of fines) leads to an increase in hardness, as in the case of unconfined yield

strength. In contrast to the shear tests though, an increase in the d_{90} (addition of coarse particles) leads to a reduction in hardness. Though the addition of coarse particles has a less significant influence on the hardness of the mixture than the addition of fine particles. The packing fraction data, shown in Fig. 27, partially explain the increased resistance to plastic deformation with the addition of fines. However, when the quantity of fines added increases the packing fraction is not greatly increased, whereas hardness is significantly affected. The mixture that has 20 % w/w fines has more contacts between fine particles, hence being more resistant to flow. In the case of the mixtures with coarse particles, the large error bars mean that firm conclusions cannot be drawn.

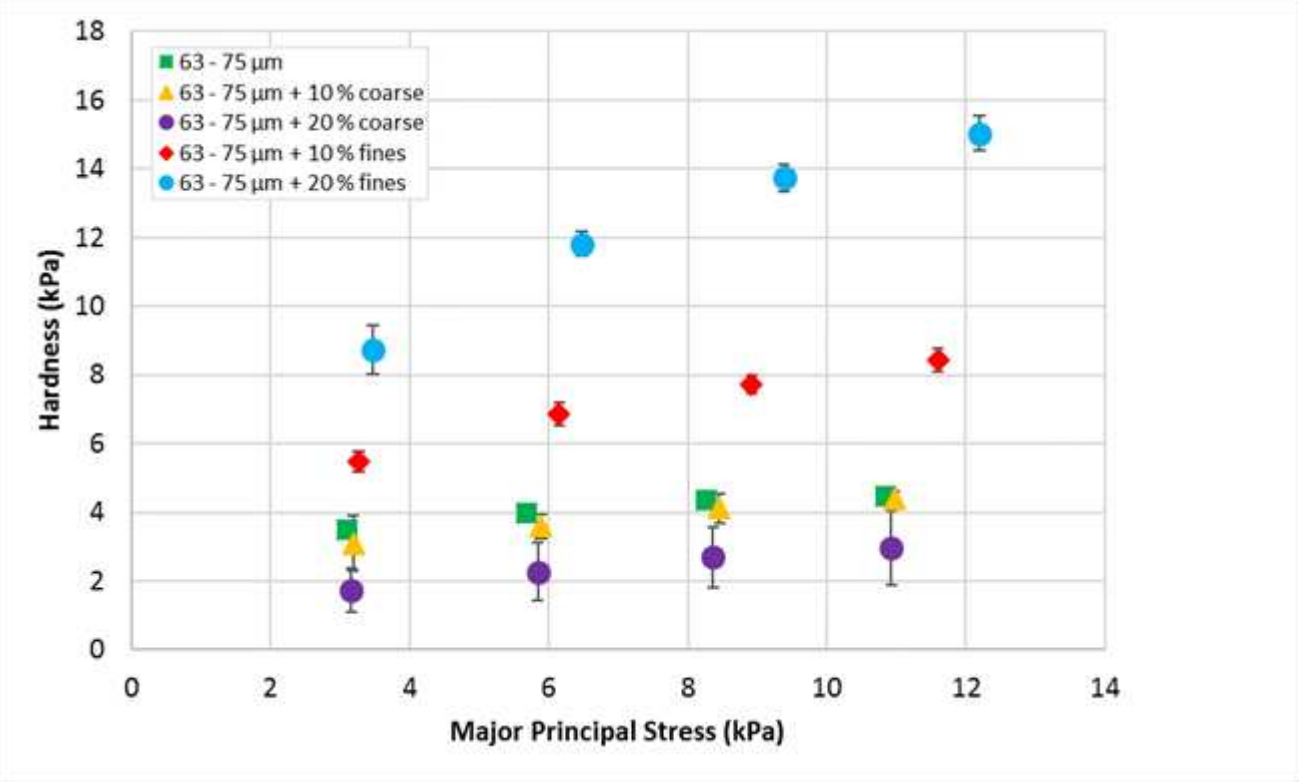

Fig. 26. Hardness as a function of major principal stress for 63 - 75 µm silanised glass beads mixed with varying amounts of coarse and fine particles, along with the 63 - 75 µm single sieve cut.

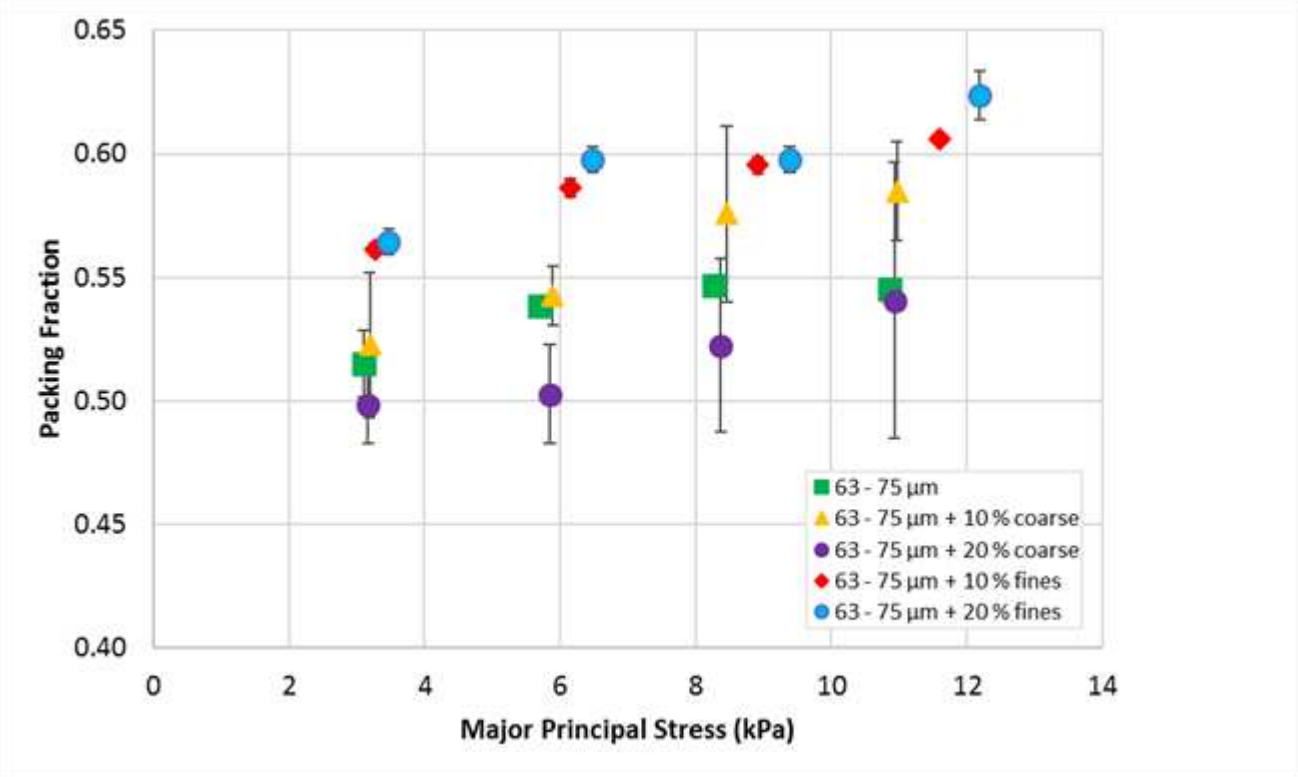

551

552 **Fig. 27.** Packing fraction as a function of major principal stress for 63 - 75 µm silanised glass beads
553 mixed with varying amounts of coarse and fine particles, along with the 63 - 75 µm single sieve cut.
554

555 The constraint factor values for the same samples with added coarse particles or fines are plotted in
556 Fig. 28, and are shown to be relatively constant regardless of stress. Moreover, as a result of the
557 trends observed in Figs. 25 and 26, *C* is found to decrease as the quantity of coarse particles in the
558 mixture is increased, while it increases as the quantity of fines in the mixture increases. Regarding
559 the glass bead mixtures studied in section 3.2.1, as size distribution is widened the d_{10} is reduced and
560 d_{90} is increased by similar amounts, so the two competing effects seen in Fig. 28 cancel each other
561 out, hence leading to only slight differences in the constraint factor between the narrow and wide
562 size distributions (see Fig. 23).

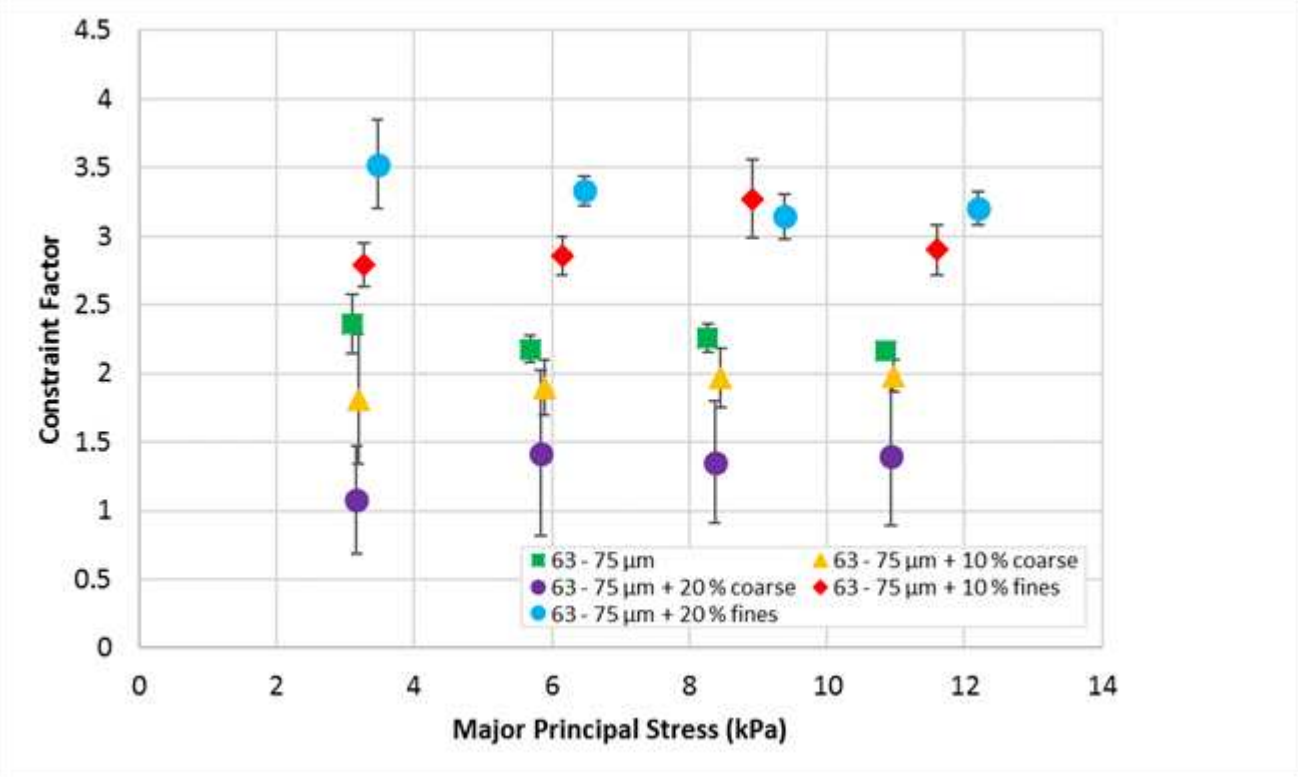

563

564 **Fig. 28.** Constraint factor as a function of major principal stress for 63 - 75 µm silanised glass beads
565 mixed with varying amounts of coarse and fine particles, along with the 63 - 75 µm single sieve cut.
566

567 In order to clearly illustrate the effect of the addition of coarse and fine particles on the constraint
568 factor, the average constraint factor values are shown for samples with added fines against d_{10} in Fig.
569 29, and with added coarse particles against d_{90} in Fig. 30. It can be seen that C decreases as either d_{10}
570 or d_{90} are increased.

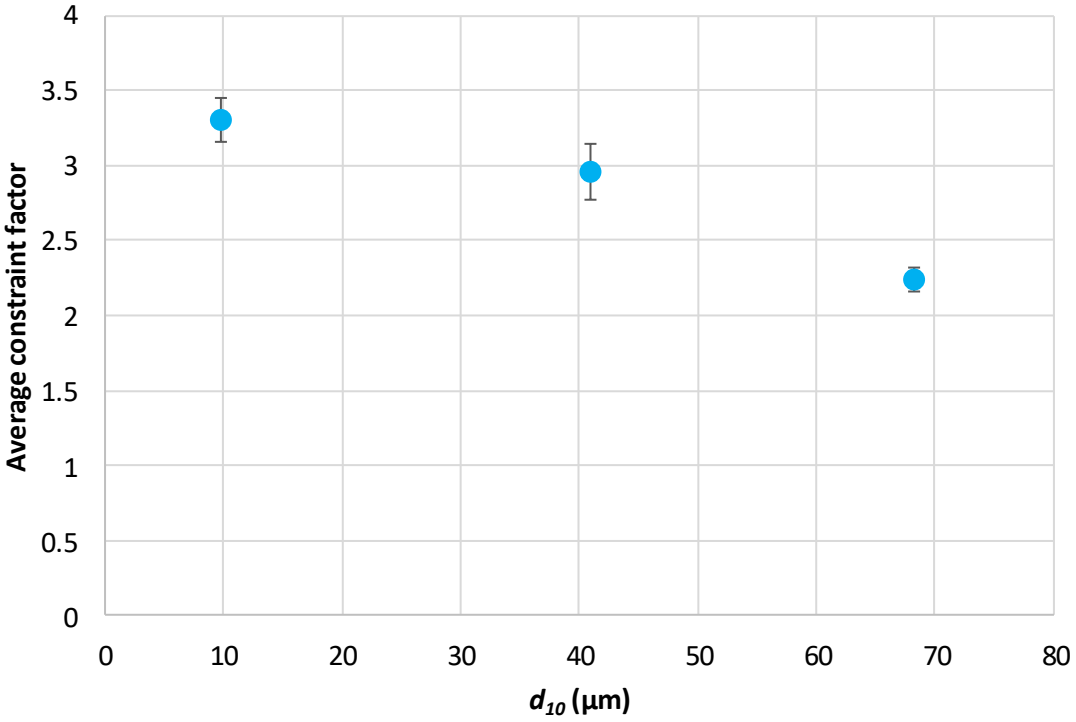

571
572

573 **Fig. 29.** Average constraint factor as a function of d_{10}.

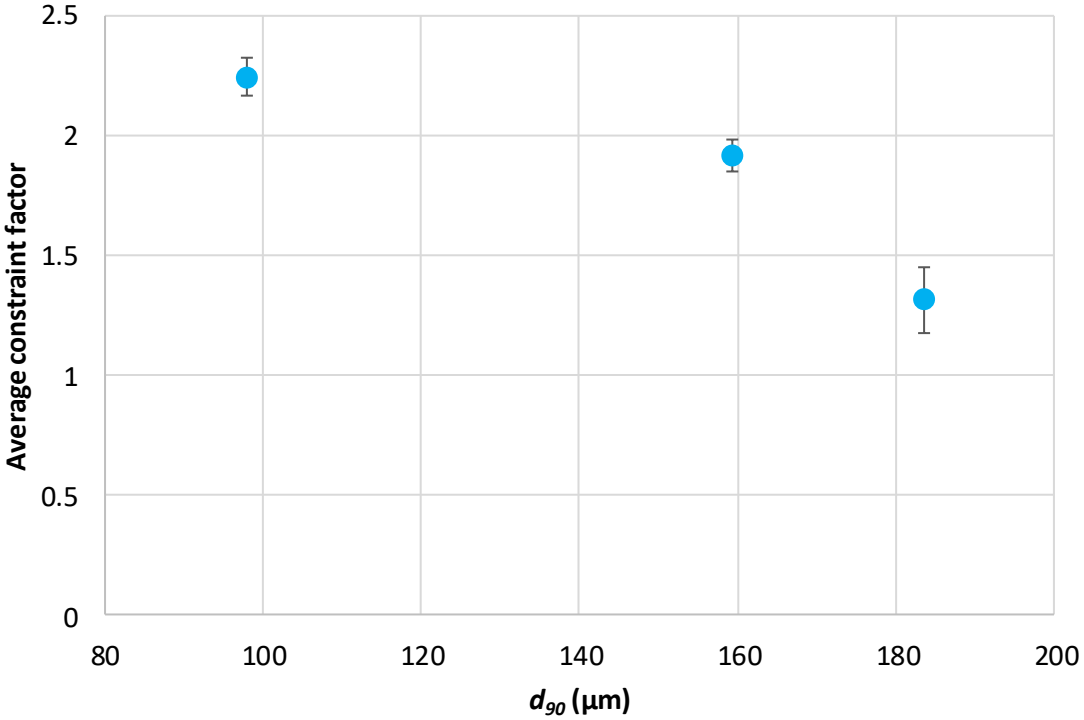

574
575

576 **Fig. 30.** Average constraint factor as a function of d_{90}.

577

4 Conclusions

The ball indentation technique was employed along with shear testing on a wide variety of glass bead samples in order to investigate the difference between powder flow behaviour at low and high stresses, and the influence of a number of size parameters (median particle size, width of size distribution, d_{10} and d_{90}) on the constraint factor and flowability.

Both unconfined yield strength and hardness were found to increase with an increase in the major principal stress applied, due to an increased packing fraction and interparticle contact area. At low stresses the increase in packing fraction with stress was more pronounced than at higher stresses, so were the hardness and unconfined yield strength measurements. Hardness was shown to be independent of penetration depth for dimensionless penetration depths between 0.3 - 0.7. The constraint factor determined from indentation and shear cell tests was virtually independent of the stress applied for all samples. As a result, the inferred unconfined yield strength from ball indentation at low stresses followed a similarly steep trend as hardness. This sharp change in behaviour at low stresses suggests that an extrapolation of shear cell results from higher stresses would overestimate the yield strength.

An increase of median particle size led to an increase in powder flowability and decrease of the constraint factor. In addition to this, widening the size distribution, while maintaining the same median size, resulted in a slight decrease of both flowability and constraint factor. The addition of fines caused a great decrease of powder flowability and an increase of constraint factor, while the addition of coarse particles appeared to only decrease the material's resistance to plastic deformation, with the unconfined yield strength being unchanged. As a result, the increase of coarse particle content led to a decrease of constraint factor.

Overall, ball indentation shows good reproducibility down to consolidation stresses of 0.1 kPa. Whereas shear cell measurements in this low stress region produce inconsistent results for this material.

603 # Acknowledgements

604 The financial support of the International Fine Particle Research Institute (IFPRI) is gratefully
605 acknowledged. Furthermore, the authors greatly appreciate the MATLAB code provided by Dr.
606 Massih Pasha (The Chemours Company) for the Warren Spring fitting of the shear cell data. The
607 authors are also thankful to Mojtaba Ghadiri and his research group at the University of Leeds for
608 the opportunity to conduct particle size measurements using the Mastersizer 2000 laser diffraction
609 instrument.

610 # References

611 [1] K. Johanson, Effect of particle shape on unconfined yield strength, Powder Technol.
612 194 (3) (2009) 246–251.
613 [2] J.K. Prescott, R.A. Barnum, On powder flowability, Pharm. Technol. 24 (10) (2000)
614 60–85.
615 [3] R.L. Carr, Classifying flow properties of solids, Chem. Eng. 1 (1965) 69–72.
616 [4] H.H. Hausner, Friction Conditions in a Mass of Metal Powder, Polytechnic Inst. of
617 Brooklyn. Univ. of California, Los Angeles, 1967.
618 [5] R. Farley, F.H.H. Valentin, Effect of particle size upon the strength of powders, Powder
619 Technol. 1 (6) (1968) 344–354.
620 [6] I.M. Wouters, D. Geldart, Characterising semi-cohesive powders using angle of repose,
621 Part. Part. Syst. Charact. 13 (4) (1996) 254–259.
622 [7] D. Geldart, E.C. Abdullah, A. Hassanpour, L.C. Nwoke, I.Wouters, Characterization of
623 powder flowability using measurement of angle of repose, China Particuology 4 (3–

624 4) (2006) 104–107.

625 [8] H. Hou, C.C. Sun, Quantifying effects of particulate properties on powder flow properties

626 using a ring shear tester, J. Pharm. Sci. 97 (9) (2008) 4030–4039.

627 [9] M. Krantz, H. Zhang, J. Zhu, Characterization of powder flow: static and dynamic

628 testing, Powder Technol. 194 (3) (2009) 239–245.

629 [10] J.J. Fitzpatrick, S.A. Barringer, T. Iqbal, Flow property measurement of food powders

630 and sensitivity of Jenike's hopper design methodology to the measured values, J.

631 Food Eng. 61 (3) (2004) 399–405.

632 [11] X. Fu, D. Huck, L. Makein, B. Armstrong, U. Willen, T. Freeman, Effect of particle

633 shape and size on flow properties of lactose powders, Particuology 10 (2) (2012)

634 203–208.

635 [12] C. Hare, M. Ghadiri, The influence of aspect ratio and roughness on flowability, AIP

636 Conf. Proc. 1542 (1) (2013, June) 887–890.

637 [13] J.M. Valverde, A. Castellanos, P.K.Watson, The effect of particle size on interparticle

638 adhesive forces for small loads, Powder Technol. 118 (3) (2001) 236–241.

639 [14] G. Lumay, F. Boschini, K. Traina, S. Bontempi, J.C. Remy, R. Cloots, N. Vandewalle,

640 Measuring the flowing properties of powders and grains, Powder Technol. 224

641 (2012) 19–27.

642 [15] E.C. Abdullah, D. Geldart, The use of bulk density measurements as flowability indicators,

643 Powder Technol. 102 (2) (1999) 151–165.

644 [16] G. Gold, R.N. Duvall, B.T. Palermo, J.G. Slater, Powder flow studies III. Factors affecting
645 the flow of lactose granules, J. Pharm. Sci. 57 (4) (1968) 667–671.
646 [17] L.X. Liu, I. Marziano, A.C. Bentham, J.D. Litster, E.T.White, T. Howes, Effect of particle
647 properties on the flowability of ibuprofen powders, Int. J. Pharm. 362 (1–2) (2008)
648 109–117.
649 [18] A. de Ryck, C. Hare, Chapter 2. Flow related properties of bulk particulate systems,
650 in: C. Hare, A. Hassanpour, M. Pasha (Eds.), Powder Flow: Theory Measurement
651 and Application, Royal Society of Chemistry, Cambridge, UK 2019, pp. 4–38.
652 [19] O. Molerus, M. Nywlt, The influence of the fine particle content of the flow behaviour
653 of bulk materials, Powder Technol. 37 (1) (1984) 145–154.
654 [20] T. Kojima, J.A. Elliott, Incipient flow properties of two-component fine powder systems
655 and their relationships with bulk density and particle contacts, Powder
656 Technol. 228 (2012) 359–370.
657 [21] A.W. Jenike, Gravity Flow of Bulk Solids, Bulletin No. 108, University of Utah, USA,
658 1961.
659 [22] A.W. Jenike, Storage and Flow of Solids, Bulletin No. 123, University of Utah, USA,
660 1964.
661 [23] D. Schulze, Powders and bulk solids, Behavior, Characterization, Storage and Flow,
662 Springer, NY, USA, 2008.
663 [24] S.V. Søgaard, T. Pedersen, M. Allesø, J. Garnaes, J. Rantanen, Evaluation of ring shear

testing as a characterization method for powder flow in small-scale powder processing equipment, Int. J. Pharm. 475 (1–2) (2014) 315–323.

[25] N. Harnby, A.E. Hawkins, D. Vandame, The use of bulk density determination as a means of typifying the flow characteristics of loosely compacted powders under conditions of variable relative humidity, Chem. Eng. Sci. 42 (4) (1987) 879–888.

[26] A. Hassanpour, M. Ghadiri, Characterisation of flowability of loosely compacted cohesive powders by indentation, Part. Part. Syst. Charact. 24 (2) (2007) 117–123.

[27] U. Zafar, C. Hare, A. Hassanpour, M. Ghadiri, Ball indentation on powder beds for assessing powder flowability: analysis of operation window, Powder Technol. 310 (2017) 300–306.

[28] M. Pasha, C. Hare, A. Hassanpour, M. Ghadiri, Analysis of ball indentation on cohesive powder beds using distinct element modelling, Powder Technol. 233 (2013) 80–90.

[29] A.G. Stavrou, C. Hare, A. Hassanpour, C.Y.Wu, Investigation of powder flowability at low stresses by DEM modelling, Chem. Eng. Sci. 211 (2020) 115307.

[30] D. Tabor, The Hardness of Metals, Oxford, UK, Oxford University Press (Clarendon Press), 1951.

[31] G.V. Kozlov, V.D. Serdyuk, V.A. Beloshenko, The plastic constraint factor and mechanical properties of a high-density polyethylene on impact loading, Mech. Compos. Mater. 30 (5) (1995) 506–509.

684 [32] U. Zafar, Assessing Flowability of Cohesive Powders by Ball Indentation, PhD Thesis
685 University of Leeds, UK, 2013.
686 [33] R. Hill, The Mathematical Theory of Plasticity, Oxford, UK, Oxford University Press
687 (Clarendon Press), 1950.
688 [34] D. Tabor, Indentation hardness: fifty years on a personal view, Philos. Mag. A 74 (5)
689 (1996) 1207–1212.
690 [35] K.L. Johnson, Contact Mechanics, Cambridge University Press, Cambridge, UK, 1985.
691 [36] C.Wang, A. Hassanpour, M. Ghadiri, Characterisation of flowability of cohesive powders
692 by testing small quantities of weak compacts, Particuology 6 (4) (2008)
693 282–285.
694 [37] M.D. Ashton, D.H. Cheng, R. Farley, F.H.H. Valentin, Some investigations into the
695 strength and flow properties of powders, Rheol. Acta 4 (3) (1965) 206–218.